12-18-2015

Paleostress States and Tectonic Evolution of the Early Mesozoic Hartford Basin

James Farrell
University of Connecticut, jamesfarrell90@gmail.com

Paleostress States and Tectonic Evolution of the Early Mesozoic Hartford Basin

James Arnold Farrell

B.S., Stony Brook University, 2012

A Thesis

Submitted in Partial Fulfillment of

the Requirements for the Degree of

Master of Science

At the

University of Connecticut

2015

APPROVAL PAGE

Masters of Science Thesis

Paleostress States and Tectonic Evolution of the Early Mesozoic Hartford Basin

Presented by

James Arnold Farrell, B.S.

Major Advisor_____
Jean M. Crespi

Associate Advisor_____
Timothy B. Byrne

Associate Advisor_____
William B. Ouimet

University of Connecticut

2015

Acknowledgements

I am considerably grateful for the support I received throughout this project. My major advisor, Dr. Jean Crespi, provided invaluable guidance and continues to be a great mentor. My associate advisors, Dr. Tim Byrne and Dr. Will Ouimet, were influential teachers and helped expand my scientific thinking. I consider my success at UConn to be a direct result of excellent advising and teaching, for that I am very thankful.

I also thank all of the community within the Center for Integrative Geosciences. The environment provided by the Center was an important foundation on which I could achieve my academic goals.

For the generous financial support, I thank the Geological Society of America, the Geological Society of Connecticut, the Billings Fund, and the Center for Integrative Geosciences.

Table of Contents

Approval Page	ii
Acknowledgements	iii
Abstract	vi
Introduction	1
Geologic Setting	3
Eastern North American Rift System	3
Central Atlantic Magmatic Province	5
Hartford Basin	6
Previous Work	7
Data	9
Fault-slip Data	9
LiDAR	12
Dike Orientations	15
Current-day Stress Orientations	17
Methods	18
Results	21
Phase 1	24
Phase 2a	25
Phase 2b	27
Phase 3	28
Phase 4	29
Discussion	31

Table of Contents

Phase 1: Doming	33
Phase 2: Drainage	34
Phase 3: Inversion	36
Phase 4: Contemporary Stress	37
Conclusions	38
References	40
Appendix A Outcrop Locations	44
Appendix B Fault-slip Data (This Study)	46
Appendix C Fault-slip Data (Clifton, 1987)	71
Appendix D Software Parameters for T-Tecto Analysis	82

Abstract

Voluminous magmatism commonly occurs during continental rifting and breakup. Along the volcanic part of the eastern North American margin, this magmatic activity is expressed by flows, dikes, and sills of the ~201 Ma Central Atlantic Magmatic Province, one of the biggest large igneous provinces in Earth history, and by seaward dipping reflectors near the continent–ocean transition, interpreted to be thick piles of breakup-related volcanic and volcaniclastic rock. The goal of this study is to identify connections between magmatic activity and crustal deformation within continental rift basins, specifically, the Hartford basin in Connecticut and Massachusetts. To accomplish this, quantitative paleostress inversion analysis was executed using 718 faults from within the basin. In addition, analysis of dike orientations, LiDAR mapping of shear zones, and data from the World Stress Map were used to determine paleostress states. The paleostress solution produced a 4-phase progression. The first phase is a normal faulting regime exhibiting radial extension, which is interpreted to be related to magmatic doming. The second phase is a composite strike-slip and normal faulting regime, interpreted to be related to drainage of CAMP magma. The third phase is a pure strike-slip compressional phase, interpreted to be related to ridge-push forces from the incipient Mid-Atlantic Ridge. The fourth phase is a pure strike-slip compressional phase, interpreted to be consistent with the current-day state of stress for the Hartford basin region. This tectonic model builds on previous studies of the Hartford basin which concluded the basin experienced 3 states of stress and did not evaluate the connections with magmatic processes. The proposed tectonic model is likely applicable to other basins along the volcanic part of the eastern North American margin.

Introduction

Rifting is one of two fundamental tectonic processes affecting continents, with the other being collision (Olsen and Morgan, 1995). Understanding the development of continental rifts and rifted margins has implications for higher order interpretations of Earth history. The Eastern North American (ENA) margin is one of the best-preserved volcanic rifted margins in the world, making it a natural laboratory for structural research using field and remote sensing methods.

Modern innovations in the field of paleostress analysis have provided new tools for geodynamic interpretations. The ability to process hundreds of faults at one time with user-controlled parameters is invaluable in testing hypotheses regarding structural and geodynamic evolution of the lithosphere. Applying this tool to the Mesozoic Hartford basin in southern New England, we have increased our understanding of volcanic rifting along the ENA margin.

The Hartford basin has a complex deformation history that has been heavily investigated by previous paleostress researchers (Clifton, 1987; de Boer and Clifton, 1988; Wise, 1981). The culmination of fault-slip research in the 1970s and 80s led to a three-phase tectonic model for the Hartford basin called "rifting-shifting-drifting" (Clifton, 1987; de Boer and Clifton, 1988; de Boer, 1992). Rifting and drifting are well-known stress states that correlate respectively with the breakup of Pangea and the current-day intraplate stresses for southern New England. Shifting, however, is an enigmatic phase consisting of strike-slip faults with a σ_1 azimuth oriented NE-SW. Some interpretations have been made about the shifting phase, though none citing known volcanic rift processes.

Many of these previous studies used analog and early computational techniques which could only analyze dozens of faults at one time. This limitation may have influenced stress constraints and geometries, thereby hindering tectonic interpretations.

Additional work in other ENA rift basins indicates a fourth phase of deformation called basin inversion (Withjack et al., 1998; Withjack et al., 2010; Withjack et al., 2012). This is a phase of post-rift compression attributed to active asthenospheric upwelling at the site of incipient seafloor spreading (Withjack et al., 1998). The σ_1 azimuth for this phase is oriented NW-SE, parallel to the initial extensional azimuth. Although this phase has been found in some ENA rift basins, it remains absent from the Hartford basin based on previous studies.

Building on previous work, this study has utilized modern computational paleostress analysis and high resolution LiDAR data to develop a new tectonic chronology for the Hartford basin. Using highly constrained paleostress geometries, along with other geologic observations, we have addressed the enigma of the "shifting" phase and the missing "inversion" phase. In addition, the cumulative paleostress results are placed in the context of volcanic rifting, providing a new evolution for the breakup of Pangea.

GEOLOGIC SETTING

Eastern North American Rift System

Rifting of Pangea in the early Mesozoic led to the formation of the eastern North American rift system, which extends from northern Florida to the Grand Banks of Canada (Fig. 1). The rift system is divided into three geographic segments on the basis of stratigraphic variations along the margin (Withjack et al., 2012). The southern segment, which includes basins in the southeastern United States, contains Upper Triassic synrift sediments. The central segment, which includes basins in the northeastern United States and southeastern Canada, contains Upper Triassic synrift sediments, CAMP flood basalts, Lower Jurassic synrift sediments, and offshore basin fill as young as the Middle Jurassic. The northern segment, which includes basins north of the Newfoundland Fracture Zone, contains Upper Triassic synrift sediments, CAMP flood basalts, and Lower Jurassic through Lower Cretaceous basin fill.

The rift system lies within the eastern North American passive margin, which is divided into volcanic and nonvolcanic sections on the basis of geophysical characteristics near the continent-ocean transition. The volcanic section contains seaward-dipping reflectors (SDRs), interpreted to be thick wedges of breakup-related volcaniclastic rocks, and a high velocity zone (HVZ), interpreted to be underplated mafic to ultramafic rocks (Austin et al., 1990; Kelemen and Holbrook, 1995). The nonvolcanic section lacks these geophysical features and has seismic transparency down to the Moho (Geoffroy, 2005). The East Coast Magnetic Anomaly is inferred to be the surface expression of the magmatic rocks at the continent-ocean transition and thus delineates the volcanic section of the eastern North American passive margin.

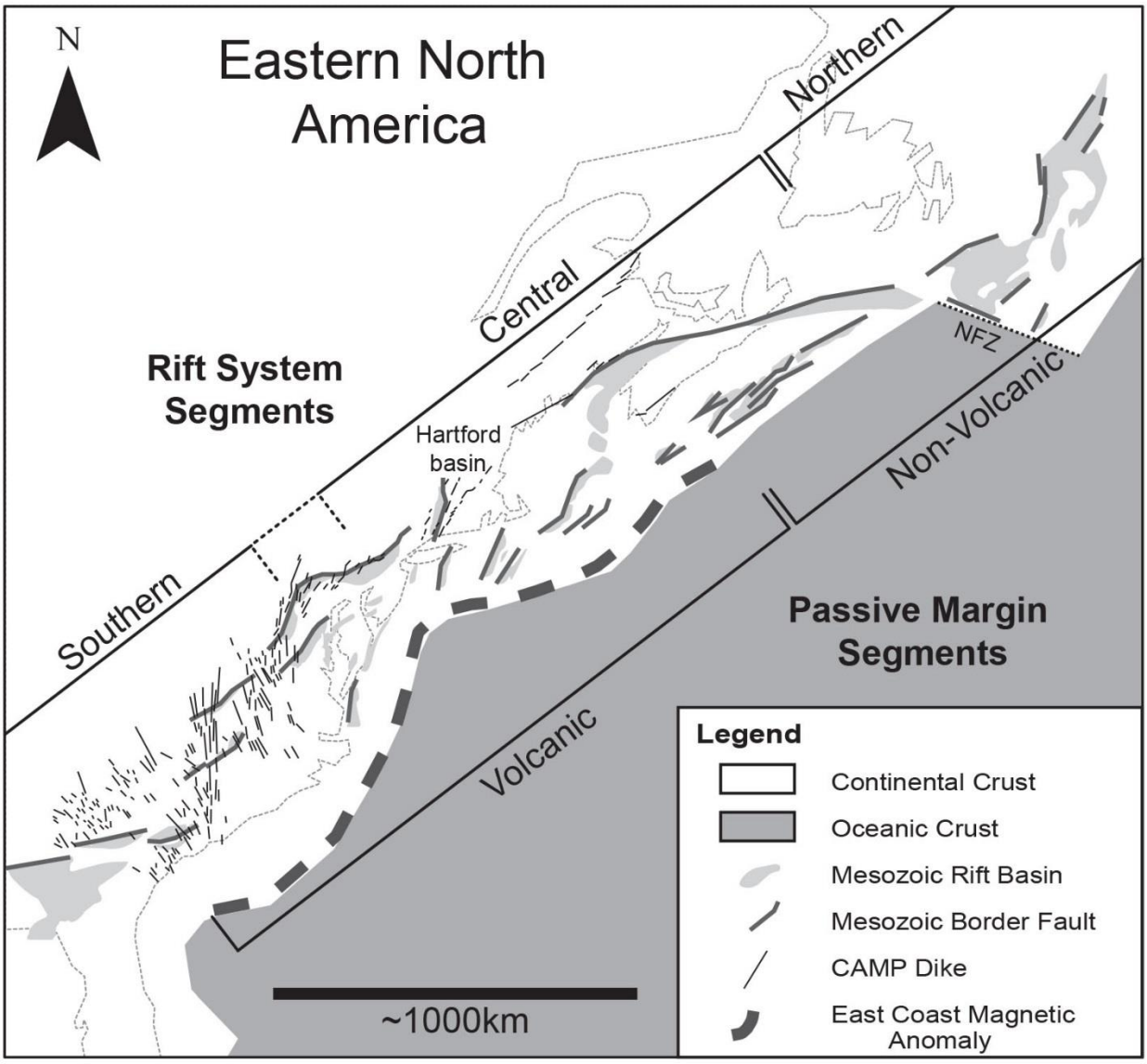

Figure 1. Simplified geologic map of eastern North American margin showing early Mesozoic rift basins and igneous features. Divisions of eastern North American rift system and eastern North American passive margin are delineated by brackets (dotted where boundary is diffuse). NFZ—Newfoundland Fracture Zone. Figure modified from Withjack et al. (2012) and McHone et al. (2014).

The boundary between the volcanic and nonvolcanic sections of the eastern North American passive margin falls within the central segment of the eastern North American rift system. The southern segment and the southern two-thirds of the central segment lie within the volcanic passive margin. The northern segment and the northern third of the central segment lie within the nonvolcanic passive margin.

Central Atlantic Magmatic Province

The Central Atlantic Magmatic Province (CAMP) is a large igneous province spanning eastern North America, northwestern Africa, northeastern South America, and Iberia (May, 1971; McHone, 2000). High-precision U/Pb geochronology indicates CAMP magmatism in eastern North America and northwestern Africa occurred at 201 Ma and had a duration of less than one million years (Blackburn et al., 2013; Schoene et al., 2010). Tholeiitic flood basalts and sills were fed by subvertical diabase dikes having a range of orientations. In eastern North America, dikes in the southern segment of the rift system trend mainly northwest whereas those in the central and northern segments trend northeast (McHone, 1988).

The timing of CAMP magmatism relative to SDR formation likely varies along the volcanic section of the margin. Rift-orthogonal dike trends and the absence of flood basalts in the rift basins of the southern segment indicate CAMP magmatism was post-rift and may have overlapped with SDR formation (Olsen et al., 2003; Withjack et al., 1998). In the volcanic part of the central segment, dike orientations and the presence of flood basalts in the synrift stratigraphy indicate CAMP magmatism occurred during rifting and therefore preceded SDR formation (Withjack et al., 1998).

Hartford Basin

The Hartford basin is located within the central segment of the eastern North American rift system, landward of the East Coast Magnetic Anomaly (Fig. 1). Two border faults bound the north-south trending basin on its east and west flanks. These faults generally parallel the Paleozoic foliation of southern New England and may be reactivated structures (Wise and Robinson, 1982). Because the Eastern Border fault was dominant during rifting, the overall structure of the basin is consistent with a half-graben. East-dipping synrift deposits are crosscut by NE-SW striking normal faults, forming several cross-grabens in the central portion of the basin. Along the eastern boundary, transverse folds are present with axes normal to the Eastern Border Fault (Schlische, 1995).

Synrift deposits of the Hartford basin consist of Upper Triassic and Lower Jurassic clastic sediments, diabase intrusions, and flood basalts (Krynine, 1950). The oldest unit, the Upper Triassic New Haven Formation, is a coarse fluvial arkose intruded by several diabase dikes and sills. Above the New Haven Formation lies the Lower Jurassic Meriden Group, which consists of three CAMP flood basalts, the Talcott, Holyoke, and Hampden basalts, and two mudstone units intercalated between the flows, the Shuttle Meadow and East Berlin formations. The CAMP basalts were fed by diabase dikes that crosscut the basin and nearby Paleozoic terranes (Philpotts and Martello, 1986). The NE-SW trending Higganum–Holden, Buttress–Ware, and Bridgeport–Pelham dikes are segmented systems that extend for over 200 km from southern Connecticut through northern Massachusetts. Above the Meriden Group lies the youngest synrift unit, the Lower Jurassic Portland Formation, a coarse fluviolacustrine arkose not crosscut by any known magmatic intrusions.

PREVIOUS WORK

In the 1970s, accelerated interest in the structural and geodynamic characteristics of the Hartford basin led to several fault-slip and fracture studies in the region (Chandler, 1978; Clifton, 1987; de Boer, 1992; de Boer and Clifton, 1988; Goldstein, 1975; Sawyer and Carroll, 1982; Wise, 1981). Initial analyses showed the structural framework of the basin reflected a complex tectonic progression not predicted by models of continental rifting.

The tectonic model, called rifting-shifting-drifting, represents three phases of deformation preserved within the Hartford basin (Clifton, 1987; de Boer and Clifton, 1988). Rifting is an extensional phase with σ_3 oriented NW-SE, representative of stresses during the early Mesozoic rifting of Pangea. Shifting is a post-rift compressional phase with σ_1 oriented NE-SW, representative of an enigmatic shift in faulting style after continental breakup. Drifting is a later post-rift compressional phase with σ_1 oriented E-W, representative of ridge-push forces and continental drift. This model explains some geodynamic characteristics of the Hartford basin, but it remains untested in the context of volcanic rift processes.

In the 1990s, studies in other eastern North American rift basins began to illuminate patterns of deformation in the context of volcanic rifting. Seismic surveys in the Fundy basin of Nova Scotia showed large reverse displacements on the border fault, along with signs of buttress folding, both cited as indicators of basin inversion (Withjack et al., 1995). Although exact paleostress axes were not originally derived, a later study including analysis of exposed structures concluded this inversion phase was produced by a σ_1 oriented NE-SW (Withjack et al., 2010). NE-SW compression is parallel to the shifting phase in the Hartford basin, but new interpretations attributed the inversion to asthenospheric upwelling and incipient ridge push forces at the time of

continental breakup. A bedrock study of rift basins in the southeastern U.S. also found inversion structures and included an interpretation of CAMP dike patterns to derive paleostress axes (Withjack et al., 1998). CAMP dike orientations in the southeastern U.S. preserved a post-rift state of stress with σ_3 oriented NE-SW and, assuming a state of horizontal compression, σ_1 oriented NW-SE. This stress orientation is nearly orthogonal to inversion-related stresses in the Hartford and Fundy basins.

If volcanic rift processes are continuous along a single rifted margin, the relative progression and geometry of the paleostress fields should be similar. NW-SE extension is accepted as the state of stress during rifting along the margin, but the orientation of basin inversion changes from north to south. In addition, a recent study of LiDAR lineaments in the Hartford basin shows structures that formed under NE-SW compression are tilted by normal faults, implying synrift origin (Martin and Evans, 2010). This is in contrast to earlier work which concluded NE-SW compression was a phase of post-rift compression (Clifton, 1987; de Boer and Clifton, 1988).

In addition, paleostress methods in the 1980s were limited to analog and early computational approaches which relied on simplifying assumptions about stress and fracturing. Despite these limitations, researchers were able to separate three prevailing paleostress states in the Hartford basin and develop a tectonic chronology explaining the associated deformational patterns.

DATA

Fault-slip Data

We analyzed 718 mesoscale faults from the Hartford basin, 180 of which were recovered from a previously published dataset (Clifton, 1987). The 538 new faults were measured at 29 outcrops throughout the basin (Fig. 2). Most of the outcrops are in the igneous units because of limited exposure of the sedimentary units. The previously published faults were measured at 17 outcrops which are clustered in four zones spanning the Western Border fault. Exact outcrop locations were not recoverable.

Fault surfaces commonly present fault-parallel laminated veins composed mainly of chlorite, calcite, and/or quartz, with fault breccia being rare. All faults have unambiguous sense of slip determined by slickenfiber steps, dilatational jogs, or drag folds. The fault-slip data are provided in Appendix B.

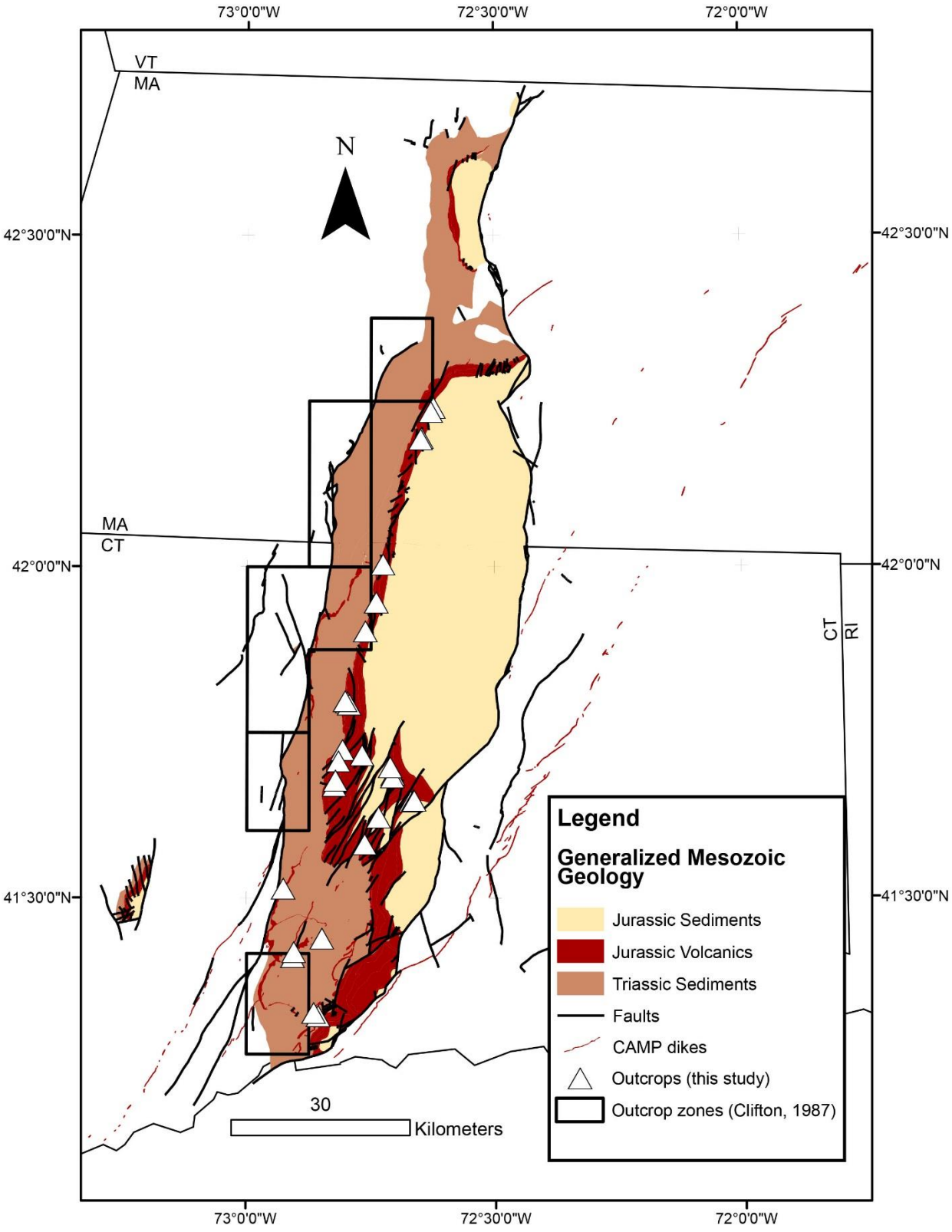

Figure 2. Generalized geologic map of early Mesozoic rift basins and CAMP dikes in central Connecticut and Massachusetts showing outcrop locations from this study and Clifton

(1987). Outcrops from this study that overlap with outcrop zones from Clifton (1987) were crosschecked to prevent redundancy.

LiDAR

LiDAR (light detection and ranging) datasets were used to construct hillshade models to illuminate large fractures in the Holyoke Basalt. In particular, we targeted regions with well-developed conjugate fracture patterns that can be used for paleostress interpretation (Fig. 3). Martin and Evans (2010) analyzed conjugate fractures cross-cutting the Holyoke Basalt in the King Philip Mountain and Ragged Mountain regions. This study includes analysis of conjugate fractures cross-cutting the Holyoke Basalt in the Hanging Hills region, in addition to those analyzed by Martin and Evans (2010). The fractures, with individual lengths exceeding 1.5 km, are interpreted to be incipient shear zones formed under NE-SW and N-S compression (Fig. 3). Ground-truthing by Martin and Evans (2010) showed that pinnate joints associated with the shear zones are perpendicular to the tilted bedding.

The dataset utilized is the CT LiDAR 10-foot survey, distributed by the University of Connecticut Center for Land Use Education and Research. Digital elevation and hillshade models used in lineament mapping were developed from point cloud data using ArcGIS.

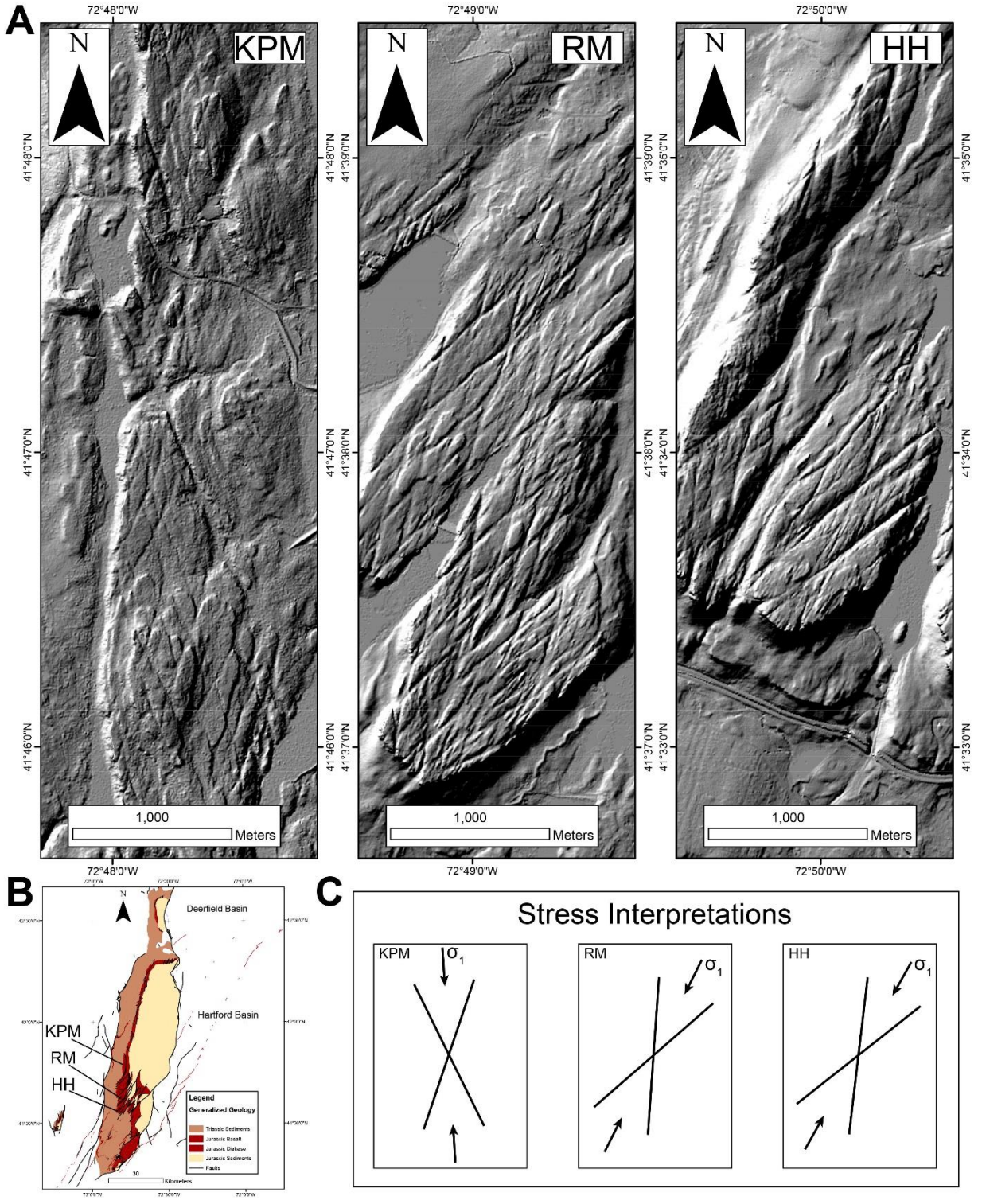

Figure 3. (A) LiDAR derived hillshade models showing X-shaped lineaments cross-cutting Holyoke Basalt in three areas of Hartford basin. KPM—King Philip Mountain, Avon, CT; RM—

Ragged Mountain, Berlin, CT; HH—Hanging Hills, Meriden, CT. (B) Generalized geologic map of Hartford basin showing locations of maps in A. (C) Generalized sketches of conjugate lineaments and associated stress interpretations. Sketches for KPM and RM modified from Martin and Evans (2010).

Dike Orientations

The orientations of the Higganum-Holden, Buttress-Ware, and Bridgeport-Pelham dike systems in Connecticut and Massachusetts were used to determine the regional orientation of σ_3 during dike intrusion associated with CAMP magmatism (Fig. 4). Igneous dikes intrude perpendicular to σ_3 in the host rock unless the intrusion follows preexisting structures (Anderson, 1951). CAMP dike segments measured in this study rarely follow preexisting structures. In addition, the overall trends of the dike systems cut obliquely across the Paleozoic terranes and the Hartford basin. Thus, σ_3 azimuths derived from the dike orientations are inferred to be representative of crustal stresses during CAMP magmatism.

Dike segment orientations were mapped using Google Earth and available digital bedrock maps for Connecticut and Massachusetts (distributed by CT DEEP and MassGIS, respectively). The trends of 263 individual dike segments were measured and averaged using a weighting system which accounts for the lengths of the segments as well as the trend. In addition, overall dike system orientations were measured and compared to the individual segments, which locally display left-stepping, en echelon geometry.

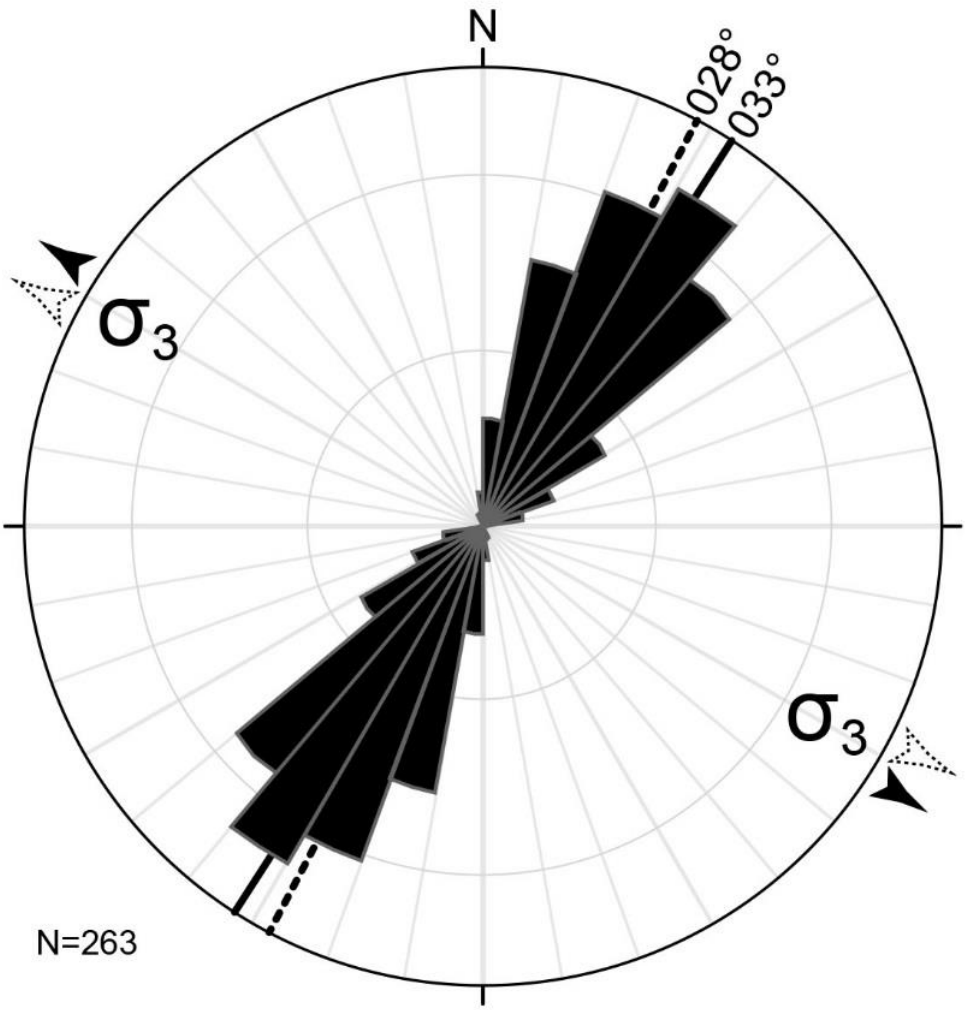

Figure 4. Rose diagram of trends of CAMP dike segments in central Connecticut and Massachusetts. Solid line—weighted average of trend of individual dike segments; dotted line—average of overall trends of Higganum–Holden, Bridgeport–Pelham, and Buttress–Ware dike systems.

Current-day Stress Orientations

Data from the 2008 World Stress Map database were used to define the current stress state in the Hartford basin region. The smoothed stress orientation map provides azimuths of maximum horizontal compression on a global grid at 0.5° spacing (Heidbach et al., 2010). These global stress values are based on earthquake focal mechanisms, borehole breakouts, in-situ measurements, and young geologic data.

Data points from the Hartford basin region yield azimuths of maximum horizontal compression ranging from 067.5° to 078.0° with an average of 072.3°. These values agree with maximum horizontal stress orientations from the nearby Moodus, Connecticut, micro-seismic zone which range from 070° to 094° (Woodward-Clyde, 1988).

METHODS

The goal of paleostress inversion is to derive a stress tensor representative of a given fault population. Because fault-slip data do not contain information on the magnitudes of the stresses, the complete stress tensor cannot be determined. Instead, paleostress inversion seeks the reduced stress tensor, which consists of the orientations of the three principal stress axes (σ_1, σ_2, σ_3) and the stress ratio ($\Phi = (\sigma_2 - \sigma_3) / (\sigma_1 - \sigma_3)$).

Paleostress inversion techniques rely on one, or both, of two assumptions. The geometric assumption states that motion along a fault is parallel to the maximum resolved shear stress on the fault surface (Bott, 1959; Wallace, 1951). The mechanical assumption states that the ratio of shear to normal stress on a fault surface exceeds the Mohr-Coulomb failure criterion (Coulomb, 1776). These assumptions, with consideration of natural variations, can be used to find the reduced stress tensor for a homogeneous fault set.

Paleostress inversion of a homogeneous fault set is relatively straightforward. Natural fault-slip datasets, however, are commonly heterogeneous and represent multiple stress states. Therefore, a parallel goal of paleostress inversion is separation of heterogeneous data into homogeneous subsets. Separation of heterogeneous fault-slip data is complex and a variety of methods have been developed, each with different separation algorithms. A review of the various methods can be found in Angelier (1994) and Célérier et al. (2012).

In this study, we use the Gauss method, executed in the software T-Tecto (Žalohar and Vrabec, 2007). This method automatically separates heterogeneous fault-slip data through a Gaussian compatibility function using both the geometric and mechanical assumptions. Maximum compatibility between a given stress tensor and fault-slip datum occurs if the slip vector parallels

the maximum resolved shear stress and the shear-to-normal stress ratio exceeds Mohr-Coulomb failure. By testing possible stress tensors against a heterogeneous dataset, T-Tecto identifies individual tensors which have a Gaussian distribution of compatibility. The tensors with optimal Gaussian compatibility are assumed to be representative of homogeneous subsets and are separated into phases in order of decreasing number of faults. Faults that cannot be explained by meaningful stress tensors are classified as misfits. Values used in this study for the paleostress inversion parameters are provided in Appendix A.

The fault-slip data from the Hartford basin were pooled in order to improve constraint on stress tensor geometry for each phase. Before pooling the data, each outcrop was analyzed for possible block rotations. Although some block rotations were identified, they are minimal and did not affect the overall results. Stress field heterogeneity was also considered before pooling the data and was determined to be insignificant. In particular, CAMP dike orientations, LiDAR shear zones, and current-day stress measurements show paleostress fields in the Hartford basin region were homogeneous for 10s to 100s of kilometers for at least four phases. Although, in principle, each outcrop should be analyzed separately (Sperner and Zweigel, 2010), no outcrop contained enough fault variety to characterize every phase.

In order to evaluate the reliability of the results of the Gauss method, two inversions were performed. The first inversion used blind separation in which the heterogeneous dataset was separated automatically into homogeneous subsets, as discussed above. In contrast, the second inversion used guided separation in which the heterogeneous dataset was separated into homogeneous subsets using known paleostress orientations from geologic data. In a study of paleostress methods, Liesa and Lisle (2004) showed that automatic separation of heterogeneous data can produce spurious results, and they recommended the inclusion of other geologic data for

correct separation of stress tensors. An advantage of T-Tecto is the preferred stress orientation function which allows the user to separate faults using defined orientations for the stress axes. The preferred stress axis orientations for the guided inversion are based on CAMP dike orientations, LiDAR shear zone orientations, and current-day stress measurements. According to these data, at least four paleostress states are preserved in the Hartford basin region.

RESULTS

Both the blind and guided inversions produced a five phase solution with minimal misfits (Fig. 5). The chronology of the phases was determined using geological observations, as discussed below. For the blind inversion, the five phases include one phase of normal faulting and four phases of strike-slip faulting. The misfits totaled approximately five percent of the dataset. For the guided inversion, the five phases include one phase of normal faulting, two phases of combined normal and strike-slip faulting, and two phases of strike-slip faulting. The misfits totaled approximately seven percent of the dataset.

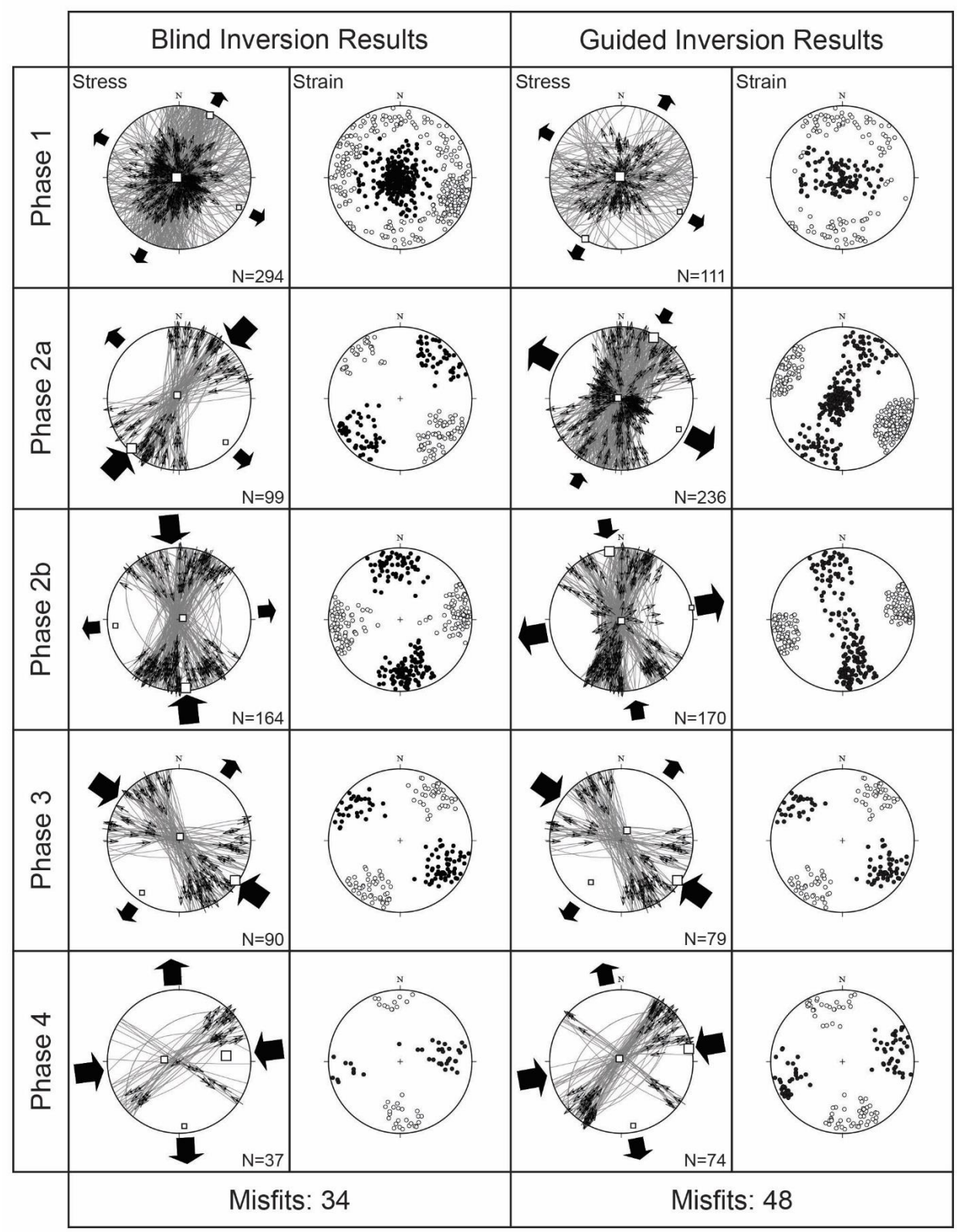

Figure 5. Results of blind and guided paleostress analyses of all fault-slip data from Hartford

basin. P- and T-axes of faults shown for comparison. Gray great circles—faults; small dot with arrow—fault striae with slip direction of hanging wall; large, medium, and small white boxes—σ_1, σ_2, and σ_3, respectively; solid black circles—P-axes; hollow circles—T-axes. Equal-angle, lower-hemisphere stereographic projections.

Phase 1

The first phase from the blind inversion yields a normal faulting stress regime with a σ_3 azimuth of 117° and a stress ratio of 0 ($\sigma_2 = \sigma_3$). The paleostress solution includes 294 normal and oblique-normal faults in a wide variety of orientations. The P-axes cluster about a vertical axis, and the T-axes form a horizontal girdle with a bias toward the southeast quadrant. Minor southeast tilting of fault blocks may account for this bias. The solution is a composite between two fault sets: one set of conjugate normal faults striking NE-SW and one set of normal and oblique-normal faults with a wide range in strikes, indicative of radial extension. This composite paleostress solution likely represents a stress permutation between σ_2 and σ_3 through time.

The first phase from the guided inversion yields a normal faulting stress regime with a σ_3 azimuth of 120° and a stress ratio of 0 ($\sigma_2 = \sigma_3$). The paleostress solution includes 111 normal and oblique-normal faults with a wide variety of orientations. The P-axes cluster about a vertical axis, and the T-axes form a partial horizontal girdle, with gaps in the east and west quadrants. Although the stress tensor geometry matches the blind inversion, the fault sets differ. The conjugate set of NE-SW striking normal faults in the blind inversion is redistributed into phases 2a and 2b because of increased compatibility with these stress tensors.

The preferred stress axis orientations for the guided inversion are based on CAMP dike trends. The weighted average trend of dike segments in Connecticut and Massachusetts is 033°, and the average of the overall trends of the three dike systems is 028° (Fig. 4). These azimuths correspond to a range of 118° to 123° for the trend of σ_3. A value of 120° for σ_3 was used for the preferred stress axis orientation with a 10° error allowance.

Geologic observations indicate this phase is the oldest phase of deformation preserved in the Hartford basin. Cross-cutting relations (Clifton, 1987) show normal faults in both inversions are cut by strike-slip faults in phase 2a. In addition, the fault set representing radial extension is most common in the Upper Triassic New Haven Formation. Faults in the NE-SW striking conjugate set, however, can be found throughout the synrift sequence. This suggests radial extension may have been a transient stage in early rifting and was later overcome by NW-SE extension.

Synrift stress regimes in the Hartford basin consistent with NW-SE extension have been documented by previous researchers (Clifton, 1987; de Boer and Clifton, 1988; Piepul, 1975; Wise, 1981). Synrift stresses representative of radial extension, however, have not been previously recognized.

Phase 2a

Phase 2a from the blind inversion yields a strike-slip faulting stress regime with a σ_1 azimuth oriented 223° and a stress ratio of 0.1. The paleostress solution includes 99 strike-slip faults in a conjugate distribution. The P-axes cluster in the NE and SW quadrants, and the T-axes cluster in the NW and SE quadrants with a bias toward the SE quadrant. Minor southeast tilting of fault blocks may account for this bias.

Phase 2a from the guided inversion yields a combined normal and strike-slip faulting stress regime with a σ_1 azimuth oriented 028° and a stress ratio of 1 ($\sigma_1 = \sigma_2$). The paleostress solution includes 236 normal and strike-slip faults. The P-axes form a girdle striking NE-SW, and the T-axes cluster in the NW and SE quadrants with a bias toward the SE quadrant. The

solution is a composite between two fault sets: one set of conjugate normal faults and one set of conjugate strike-slip faults. This composite paleostress solution likely represents a stress permutation between σ_1 and σ_2 through time. Similar stress permutations between normal and strike-slip faulting have been recognized in the Basin and Range province (Angelier et al., 1985).

The preferred stress axis orientations for the guided inversion are based on conjugate LiDAR shear zones in the Holyoke Basalt. At Ragged Mountain and the Hanging Hills, shear zone strikes average 015° and 050° with an average bisect trend of 032.5° (Fig. 3) (Martin and Evans, 2010). This bisect trend is assumed to be parallel to σ_1 during shear zone formation. A σ_1 value of 033° is used for the preferred stress axis orientation with a 10° error allowance. Although the shear zones are tilted to the southeast, the tilt is less than 15° and not a factor in determining strikes in map view.

Both inversions have a component of NE-SW strike-slip compression which is consistent with previous work (Clifton, 1987; de Boer, 1992; de Boer and Clifton, 1988; Wise, 1981). NE-SW compression is cited as the shifting phase in the rifting-shifting-drifting tectonic model (Clifton, 1987; de Boer and Clifton, 1988). The composite normal and strike-slip faulting stress regime from the guided inversion, however, is inconsistent with previous work, which concluded that normal faulting related to NW-SE extension and strike-slip faulting related to NE-SW compression occurred in separate phases of deformation (Clifton, 1987; de Boer and Clifton, 1988). Geologic observations support the composite stress regime of the guided inversion. Tilting of strike-slip faults and LiDAR shear zones implies normal faulting followed strike-slip faulting, whereas vertical strike-slip faults imply the opposite progression. This indicates multiple permutations of σ_1 and σ_2 through time and, as a result, a composite phase of deformation.

Phase 2b

Phase 2b from the blind inversion yields a strike-slip faulting stress regime with a σ_1 azimuth oriented 174° and a stress ratio of 0.1. The paleostress solution includes 164 strike-slip faults in a conjugate distribution. The P-axes cluster in the N and S quadrants, and the T-axes cluster in the W and E quadrants.

Phase 2b from the guided inversion yields a composite normal and strike-slip faulting stress regime with a σ_1 azimuth oriented 350° and a stress ratio of 1 ($\sigma_1 = \sigma_2$). The paleostress solution includes 170 normal and strike-slip faults, both with conjugate distributions. The P-axes form a girdle striking N-S, and the T-axes cluster in the W and E quadrants. Similar to phase 2a, this composite paleostress solution likely represents a stress permutation between σ_1 and σ_2 through time.

The preferred stress axis orientations for the guided inversion are based on conjugate LiDAR shear zones in the Holyoke Basalt. At King Philip Mountain, shear zone strikes average 340° and 020° with an average bisect trend of 000° (Fig. 3) (Martin and Evans, 2010). This bisect trend is assumed to be parallel to σ_1 during shear zone formation. A σ_1 value of 000° is used for the preferred stress axis orientation with a 10° error allowance. Although the shear zones are tilted to the east, the tilt is less than 15° and not a factor in determining strikes in map view.

No cross-cutting relations are available for faults in phase 2b, but striking similarities between phases 2a and 2b suggest they are coeval. Paleostress solutions from the guided inversion for phases 2a and 2b both show composite normal and strike-slip faulting stress

regimes. In addition, conjugate LiDAR shear zones in King Philip Mountain have nearly the same appearance as the Ragged Mountain and Hanging Hills shear zones, but with a moderate difference in orientation. Shear zones in the latter regions are bounded, and likely tilted by, NE-SW striking normal faults, whereas shear zones in the King Philip Mountain region are present in the tilted hanging wall of a N-S striking normal fault. The same geometries are observed at the mesoscale. The vast majority of faults from phase 2b were measured at three outcrops, and these faults likely represent a variant of the more prevailing phase 2a. The larger number of faults in phase 2b relative to phase 2a is due to a sampling bias. Local zones of N-S strike-slip compression in the Hartford basin have been previously documented and attributed to complex block rotations (Wise, 1981).

Phase 3

Phase 3 from the blind inversion yields a strike-slip faulting stress regime with a σ_1 azimuth oriented 125° and a stress ratio of 0.1. The paleostress solution includes 90 strike-slip faults in a conjugate distribution. The P-axes cluster in the NW and SE quadrants, and the T-axes cluster in the NE and SW quadrants.

Phase 3 from the guided inversion yields a similar strike-slip faulting stress regime with a σ_1 azimuth oriented 125° and a stress ratio of 0.1. The paleostress solution includes 79 strike-slip faults in a conjugate distribution. The P-axes cluster in the NW and SE quadrants, and the T-axes cluster in the NE and SW quadrants. This solution is nearly identical to the blind inversion, differing only in number of faults.

No preferred stress axis orientation was used for phase 3 in the guided inversion because no map-scale geologic evidence was found for NW-SE compression. Therefore, phase 3 results are representative of the blind inversion technique. Slight differences in results between the blind and guided solutions are due to processing order. In the guided inversion, phase 3 was processed last, so a slight redistribution of data led to a smaller number of compatible faults.

P and T axes and fault orientations from phase 3 show no indication of tilting, suggesting this phase postdates normal faulting associated with phases 1, 2a, and 2b. In addition, phase 3 is inferred to predate phase 4, which is assumed to be the current day stress state. No direct cross-cutting relations were found involving faults from phase 3.

NW-SE compression has not previously been identified in the Hartford basin. However, phase 3 stress orientations and relative chronology are consistent with observations in the southern segment of the eastern North American rift system, where basin inversion has been inferred to be a result of post-rift compression oriented NW-SE (Withjack et al., 1998, 2012). In Connecticut, NW-SE compression was documented in a study of the Higganum dike, but was misinterpreted as the contemporary stress state for southern New England (Sawyer and Carroll, 1982).

Phase 4

Phase 4 from the blind inversion yields a strike-slip faulting stress regime with a σ_1 azimuth oriented 083° and a stress ratio of 0.4. The paleostress solution includes 37 strike-slip faults. The P-axes cluster in the W and E quadrants, and the T-axes cluster in the N and S

quadrants, with a slight bias toward the S quadrant. The low number of faults may account for this bias.

Phase 4 from the guided inversion yields a strike-slip faulting stress regime with a σ_1 azimuth oriented 079° and a stress ratio of 0.3. The paleostress solution includes 74 strike-slip faults. The P-axes cluster in the W and E quadrants, and the T-axes cluster in the N and S quadrants. Unlike the blind inversion, T-axes show no bias in orientation. Differences in fault numbers between solutions are due to processing order. In the blind inversion, phase 4 was processed last, so a slight redistribution of data led to a smaller number of compatible faults.

The preferred stress axis orientation for the guided inversion is based mapping of current day stress in central Connecticut and Massachusetts. Azimuths of maximum horizontal compression from the World Stress Map smoothed grid range from 068° to 078° for the Hartford basin region (Heidbach et al., 2010). Azimuths of maximum horizontal compression from a study of the nearby micro-seismic zone in Moodus, Connecticut, range from 070° to 094° (Woodward-Clyde, 1988). These azimuths are assumed to be parallel to σ_1, and, in order to cover both ranges, a median value of 081° for σ_1 was used with an error allowance of 15°.

Phase 4 is assumed to be the youngest phase of deformation. Although mapping of current day stress in the Hartford basin region indicates a thrust-faulting stress regime, strike-slip faults in phase 4 formed under a parallel azimuth of maximum compression. This stress state is proposed to have originated as early as the Cretaceous (de Boer, 1992; Manning and de Boer, 1989).

DISCUSSION

Using the paleostress inversion results and other geologic observations, we propose a new tectonic model for the evolution of the Hartford basin. This model embeds tectonic interpretations within the context of volcanic passive margin development. In addition, we interpret the interplay between magmatic processes and crustal deformation during the synrift and breakup stages. The proposed dynamics may have affected the nearby Newark and Fundy basins, which are similar in both structure and stratigraphy. The model may as well apply to the southern segment of the eastern North American rift system, if not with different timing. Furthermore, there may be implications for uniformity in the formation of volcanic passive margins around the world.

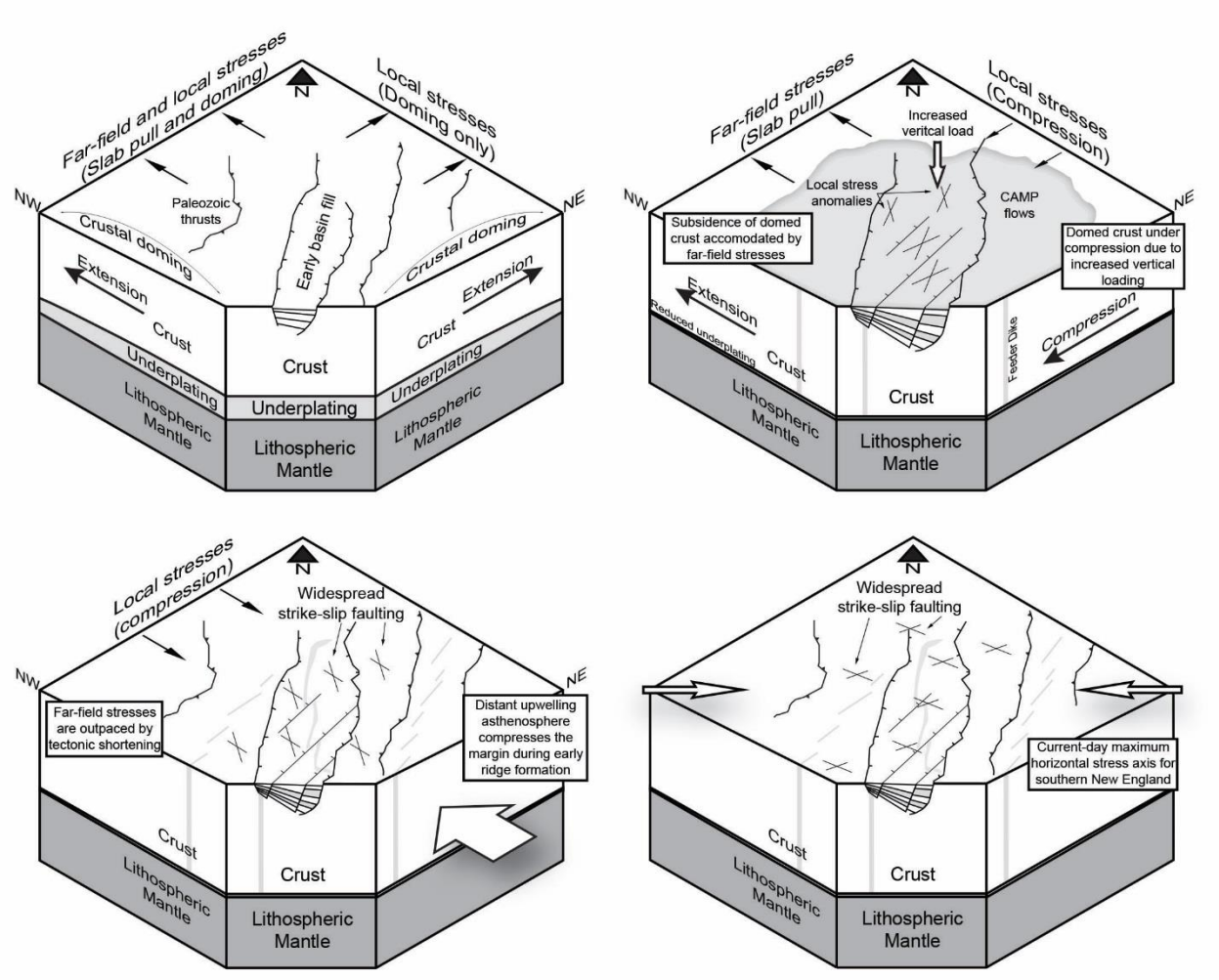

Figure 6. Block diagrams of proposed tectonic model for Hartford basin. (A) Phase 1—doming. (B) Phase 2—drainage. (C) Phase 3—inversion. (D) Phase 4—drifting.

Phase 1: Doming

Phase 1 is interpreted to be the first phase of tectonic deformation affecting the Hartford basin. The paleostress fields in this phase are likely representative of the initiation of rifting in the central segment of the Eastern North American rift system. Deformation in phase 1 is interpreted to be a result of two interacting stress fields with two independent fault sets. The exact regime may have been a complex composite stress system, but the fault sets are treated separately for interpretation purposes.

Fault set one is indicative of NW-SE extension by conjugate normal faulting. As previously discussed, fault set one can be found throughout the synrift sequence and likely represents passive extension by slab pull stresses. Slab-pull influence may have lasted from initiation of rifting until breakup, but was overprinted periodically by stresses related to local magmatic processes.

Fault set two is indicative of radial extension with no preferred fault orientation. This fault set is interpreted to be a result of transient magmatic doming, a precursor to the Central Atlantic Magmatic Province. Isostatic forces related to CAMP magma reservoirs, and possibly an upper mantle thermal anomaly, likely drove lower crustal convection and surface uplift. Outward flow of the magmatic dome resulted in a low stress ratio ($\sigma_2 \simeq \sigma_3$), causing upper crustal normal faults to form in a variety of orientations. Stresses and deformation from the emplacement of this dome would have ended after the eruption of CAMP magma. This is consistent with observations that indicate radial normal faults are found mostly in the oldest synrift sediments and are not found in post-CAMP sediments.

Crustal doming has been recognized in continental rift environments and large igneous provinces. Some studies suggest doming is related to mantle plumes (Bonini et al., 2005; Bott,

1981, 1992; Holbrook et al., 2001; Huismans et al., 2001; Saunders et al., 2007) and others suggest doming is related to magmatic reservoir processes (Brodie and White, 1994; McHone et al., 2005; Silver et al., 2006; Sue et al., 2014; Ziegler and Cloetingh, 2004). In the case of Pangean rifting, no physical evidence is available for a mantle plume near the Hartford basin (McHone, 2000; McHone et al., 2005). Therefore, lithospheric magmatism is a more likely cause for the regional doming stress acting in superposition with the far-field slab-pull. It is possible this magmatism is related to mafic crustal underplating during early continental rifting.

Phase 2: Drainage

Phase 2 is the second phase of rifting, which is inferred to have initiated at the time of CAMP volcanism in the latest Triassic–earliest Jurassic. During this phase, NW-SE extension was still acting, but radial extension from doming was subsiding. The drainage of magma reservoirs onto the surface increased the vertical loading stress on the crustal dome. This dome, which was extended by normal faulting, was vertically compressed and collapsed through the drainage of CAMP basalts onto the surface. The increased vertical load and drainage of magma reservoirs began to flatten the dome. Extension in the NW-SE direction was accommodated by the pervasive far-field stresses; however, extension in the NE-SW direction was replaced by shortening as a result of flattening of the crustal dome. Previously, extension in the NE-SW direction was accommodated by doming, which was no longer active during CAMP. Therefore, flattening of the crustal dome resulted in a relative compression oriented NE-SW.

The drainage mechanism has been used to explain flood basalt occurrences in cratonic regions (Silver et al., 2006). A two stage model was proposed that explained the formation and

subsequent drainage of lithospheric magma reservoirs in stable cratons (Silver et al., 2006). The drainage process appears to have been similar for the eastern North American rift system based on two fundamental observations. First, CAMP volcanics were fed by subcrustal magmatic reservoirs (McHone et al., 2005; McHone et al., 2014). Second, these reservoirs drained on to the surface in less than one million years (Olsen et al., 2003; Olsen et al., 1996). This rapid magmatic drainage impacted the state of stress in the Hartford basin and possibly the nearby Newark and Fundy basins.

Regional strain during this phase was no longer accommodated by the inherited structural grain. Instead, NE-SW striking normal faults cross-cut the N-S trending basin and formed a series of cross grabens that cross-cut all synrift units. In some localities, cross grabens are bounded by N-S striking normal faults with geometries similar to faults in phase 2b of the guided paleostress inversion. These are thought to be local anomalies related to stress perturbations or complex block rotation (Wise, 1981).

Previous studies have proposed that NE-SW compression was a post-rift state of stress (Clifton, 1987; de Boer, 1992; de Boer and Clifton, 1988; Manning and de Boer, 1989; Withjack et al., 2012). This study proposes NE-SW compression is synrift and related to CAMP volcanism. The drainage of CAMP magmatic reservoirs explains the coeval origin of normal and strike-slip faults in phase 2a of the guided paleostress inversion. The phase 2a stress tensor shows σ_3 was consistently oriented NW-SE, but σ_1 alternated between vertical and NE-SW. This permutation also explains the occurrence of tilted incipient shear zones in the Holyoke Basalt which formed under subhorizontal NE-SW compression. A similar progression from strike-slip to normal faulting was observed in the adjacent Deerfield basin (Goldstein, 1975). The sharing of a principal stress axis and tilting of compressional structures suggest late stage rifting was accommodated by both normal and strike-slip faulting.

Phase 3: Inversion

Phase 3 is interpreted to be the first post-rift state of stress for the Hartford basin and is inferred to be marked by the transition from rifting to seafloor spreading in the central segment of the eastern North American rift system. By this time, volcanic processes previously affecting the Hartford basin had ceased. At the site of incipient seafloor spreading, active upwelling of the asthenosphere created a compressive stress that affected the newly formed continental margins (Withjack et al., 1998). The North American continent was still under slab-pull influence; however, this passive displacement was outpaced by the asthenospheric compression. This mechanism resulted in a horizontal σ_1 oriented NW-SE, parallel to the initial σ_3 direction for rifting.

The inversion phase was elusive in the central segment of the margin because no large-scale structures preserve this stress state. In the southern segment, CAMP dike orientations and map-scale thrusts preserve the evidence for basin inversion (Withjack et al., 1998). Because of the diachronous nature of Atlantic rifting, CAMP dike orientations in the central segment preserve synrift stresses (Withjack et al., 1998, 2012).

Although this phase has not been reported in the Hartford basin, NW-SE compression was previously identified from an early paleostress study of the Higganum dike (Sawyer and Carroll, 1982). These results were interpreted to be correlative with the current day state of stress, which was not well constrained at the time. Later reports indicate the current day state of stress for southern New England is E-W compression (Hurd and Zoback, 2012; Woodward-Clyde, 1988; Zoback, 1992). NW-SE compression in the Higganum dike may be related to the basin inversion phase.

Phase 4: Contemporary Stress

Phase 4 is interpreted to be the most recent state of stress preserved in the Hartford basin. Both paleostress methods indicate E-W compression, which is consistent with studies of contemporary stress in southern New England (Heidbach et al., 2010; Hurd and Zoback, 2012; Woodward-Clyde, 1988; Zoback, 1992). This phase followed the inversion phase and persisted throughout seafloor spreading. The transition occurred when active asthenospheric upwelling gave way to passive asthenospheric upwelling (Withjack et al., 1998). Once oceanic lithosphere began to form, forces such as ridge-push and asthenospheric drag compressed the newly formed passive margins (Hurd and Zoback, 2012; Zoback, 1992).

Paleostress results from phase 4 indicate strike-slip faulting, but mapping of current day stress indicates most of the northeastern United States in a thrust regime (Hurd and Zoback, 2012; Zoback, 1992). Focal mechanism solutions from the nearby Moodus microseismic zone also show a thrust faulting regime (Ebel, 1989; Woodward-Clyde, 1988). The Hartford basin region is currently in a thrust setting. Therefore, a transition must have occurred to accommodate the stress permutation. One hypothesis for this permutation mechanism is a decrease in vertical loading stress from glacial processes. Laurentide glaciation in North America removed bedrock and surficial cover, replacing it with low-density glacial deposits. This change in upper crustal material density may have decreased the gravitational loading stress. If σ_2 and σ_3 were close in relative magnitude before glaciation, the decreased loading may have caused a $\sigma_2 - \sigma_3$ stress permutation, changing a strike-slip faulting regime to a thrust faulting regime.

CONCLUSIONS

Modern paleostress analysis of faults from the Hartford basin reveals a four-phase stress model that can be explained by volcanic rift processes. The first phase is characterized by radial extension caused by magmatic doming and far-field slab-pull. The second phase is characterized by alternating stages of NW-SE extension and NE-SW compression, a consequence of CAMP volcanism. The third phase is a post-rift inversion caused by active asthenospheric upwelling; as a result, the margin was compressed in a NW-SE direction. The fourth phase is consistent with ridge-push and asthenospheric drag, compressing the margin in an E-W direction.

One significant contribution of this analysis is the connection between NE-SW compression and NW-SE extension. Previously, this shifting phase was interpreted to be a post-rift state of stress (Clifton, 1987; de Boer and Clifton, 1988). Modern paleostress and LiDAR analysis shows that some NE-SW compressional structures are tilted, indicating a synrift origin.

Additionally, the discovery of NW-SE compression in the Hartford basin has added clarity to the tectonic evolution of the Eastern North American margin. NW-SE compression, or basin inversion, was previously found only in the southern segment of the margin (Withjack et al., 2012). Considering the central and southern segments are both volcanic margins, the deformation patterns should be similar. The discovery of inversion in the Hartford basin suggests the two margins developed similarly in terms of relative tectonic chronology.

Building upon previous paleostress work, this new tectonic chronology for the Hartford basin presents an evolution in the context of volcanic rifting. New techniques in computational paleostress and high resolution LiDAR availability provided a framework for advanced tectonic

investigation. This type of analysis may be useful in other Eastern North American rift basins in order to test regional consistency and/or variations in tectonic evolution along the margin.

References

Anderson, E. M., 1951, The dynamics of faulting and dyke formation with applications to Britain, Hafner Pub. Co.

Angelier, J., 1994, Fault slip analysis and paleostress reconstruction: Continental deformation, v. 4, p. 101-120.

Angelier, J., Colletta, B., and Anderson, R. E., 1985, Neogene paleostress changes in the Basin and Range: A case study at Hoover Dam, Nevada-Arizona: Geological Society of America Bulletin, v. 96, no. 3, p. 347-361.

Austin, J. A., Stoffa, P. L., Phillips, J. D., Oh, J., Sawyer, D. S., Purdy, G. M., Reiter, E., and Makris, J., 1990, Crustal structure of the Southeast Georgia embayment-Carolina Trough: Preliminary results of a composite seismic image of a continental suture (?) and a volcanic passive margin: Geology, v. 18, no. 10, p. 1023-1027.

Blackburn, T. J., Olsen, P. E., Bowring, S. A., McLean, N. M., Kent, D. V., Puffer, J., McHone, G., Rasbury, E. T., and Et-Touhami, M., 2013, Zircon U-Pb geochronology links the end-Triassic extinction with the Central Atlantic Magmatic Province: Science, v. 340, no. 6135, p. 941-945.

Bonini, M., Corti, G., Innocenti, F., Manetti, P., Mazzarini, F., Abebe, T., and Pecskay, Z., 2005, Evolution of the Main Ethiopian Rift in the frame of Afar and Kenya rifts propagation: Tectonics, v. 24, no. 1.

Bott, M., 1981, Crustal doming and the mechanism of continental rifting: Tectonophysics, v. 73, no. 1, p. 1-8.

-, 1992, The stress regime associated with continental break-up: Geological Society, London, Special Publications, v. 68, no. 1, p. 125-136.

Bott, M. H. P., 1959, The mechanics of oblique slip faulting: Geological Magazine, v. 96, no. 02, p. 109-117.

Brodie, J., and White, N., 1994, Sedimentary basin inversion caused by igneous underplating: Northwest European continental shelf: Geology, v. 22, no. 2, p. 147-150.

Célérier, B., Etchecopar, A., Bergerat, F., Vergely, P., Arthaud, F., and Laurent, P., 2012, Inferring stress from faulting: from early concepts to inverse methods: Tectonophysics, v. 581, p. 206-219.

Chandler, W., 1978, Graben mechanics at the junction of the Hartford and Deerfield basins of the Connecticut Valley [M.S.: University of Massachusetts.

Clifton, A. E., 1987, Tectonic analysis of the western border fault zone of the Mesozoic Hartford Basin, Connecticut and Massachusetts [M.A.

Coulomb, C. A., 1776, Essai sur une application des règles de maximis & minimis à quelques problèmes de statique, relatifs à l'architecture, De l'Imprimerie Royale.

de Boer, J., 1992, Stress configurations during and following emplacement of ENA basalts in the northern Appalachians: Geological Society of America Special Papers, v. 268, p. 361-378.

de Boer, J., and Clifton, A., 1988, Mesozoic tectogenesis: Development and deformation of "Newark" rift zones in the Appalachians (with special emphasis on the Hartford basin, Connecticut), Triassic-Jurassic rifting: New York, Elsevier, p. 275-306.

Ebel, J. E., 1989, A comparison of the 1981, 1982, 1986 and 1987–1988 microearthquake swarms at Moodus, Connecticut: Seismological Research Letters, v. 60, no. 4, p. 177-184.

Geoffroy, L., 2005, Volcanic passive margins: Comptes Rendus Geoscience, v. 337, no. 16, p. 1395-1408.

Goldstein, A. G., 1975, Brittle fracture history of the Montague Basin, northcentral Massachusetts [M.S.: University of Massachusetts, 108 p.

Heidbach, O., Tingay, M., Barth, A., Reinecker, J., Kurfeß, D., and Müller, B., 2010, Global crustal stress pattern based on the World Stress Map database release 2008: Tectonophysics, v. 482, no. 1, p. 3-15.

Holbrook, W. S., Larsen, H., Korenaga, J., Dahl-Jensen, T., Reid, I. D., Kelemen, P., Hopper, J., Kent, G., Lizarralde, D., and Bernstein, S., 2001, Mantle thermal structure and active upwelling during continental breakup in the North Atlantic: Earth and Planetary Science Letters, v. 190, no. 3, p. 251-266.

Huismans, R. S., Podladchikov, Y. Y., and Cloetingh, S., 2001, Transition from passive to active rifting: Relative importance of asthenospheric doming and passive extension of the lithosphere: Journal of Geophysical Research: Solid Earth (1978–2012), v. 106, no. B6, p. 11271-11291.

Hurd, O., and Zoback, M. D., 2012, Intraplate earthquakes, regional stress and fault mechanics in the Central and Eastern US and Southeastern Canada: Tectonophysics, v. 581, p. 182-192.

Kelemen, P. B., and Holbrook, W. S., 1995, Origin of thick, high-velocity igneous crust along the US East Coast Margin: Journal of Geophysical Research: Solid Earth (1978–2012), v. 100, no. B6, p. 10077-10094.

Krynine, P. D., 1950, Petrology, stratigraphy, and origin of the Triassic sedimentary rocks of Connecticut, State Geological and Natural History Survey, v. 73.

Liesa, C. L., and Lisle, R. J., 2004, Reliability of methods to separate stress tensors from heterogeneous fault-slip data: Journal of structural geology, v. 26, no. 3, p. 559-572.

Manning, A. H., and de Boer, J. Z., 1989, Deformation of Mesozoic dikes in New England: Geology, v. 17, no. 11, p. 1016-1019.

Martin, T. E., and Evans, M., Brittle Structures In The Holyoke Basalt Of The Hartford Basin: Ground-Truthing LiDAR Linears, *in* Proceedings Geological Society of America Abstracts with Programs2010, Volume 42, p. 85.

May, P. R., 1971, Pattern of Triassic-Jurassic diabase dikes around the North Atlantic in the context of predrift position of the continents: Geological Society of America Bulletin, v. 82, no. 5, p. 1285-1292.

McHone, J. G., 1988, Tectonic and paleostress patterns of Mesozoic intrusions in eastern North America: Triassic–Jurassic rifting, continental breakup and the origin of the Atlantic Ocean passive margins, part A: New York, Elsevier, p. 608-620.

-, 2000, Non-plume magmatism and rifting during the opening of the central Atlantic Ocean: Tectonophysics, v. 316, no. 3, p. 287-296.

McHone, J. G., Anderson, D. L., Beutel, E. K., and Fialko, Y. A., 2005, Giant dikes, rifts, flood basalts, and plate tectonics: A contention of mantle models: Geological Society of America Special Papers, v. 388, p. 401-420.

McHone, J. G., Hussey, A. M., West, D. P., and Bailey, D. G., 2014, The Christmas Cove Dyke of coastal Maine, USA, and regional sources for Early Mesozoic flood basalts in northeastern North America: Atlantic Geology, v. 50, p. 66-90.

Olsen, K., and Morgan, P., 1995, Introduction: progress in understanding continental rifts, *in* Olsen, K., ed., Continental Rifts: Evolution, Structure, Tectonics, Volume 25, El Sevier, p. 3-26.

Olsen, P. E., Kent, D. V., Et-Touhami, M., and Puffer, J., 2003, Cyclo-, magneto-, and bio-stratigraphic constraints on the duration of the CAMP event and its relationship to the

Triassic-Jurassic Boundary: The Central Atlantic Magmatic Province: Insights from Fragments of Pangea, p. 7-32.
Olsen, P. E., Schlische, R. W., and Fedosh, M. S., 1996, 580 ky duration of the Early Jurassic flood basalt event in eastern North America estimated using Milankovitch cyclostratigraphy: The Continental Jurassic, Museum of Northern Arizona Bulletin, v. 60, p. 11-22.
Philpotts, A. R., and Martello, A., 1986, Diabase feeder dikes for the Mesozoic basalts in southern New England: American Journal of Science, v. 286, no. 2, p. 105-126.
Piepul, R. G., 1975, Analysis of jointing and faulting at the southern end of the Eastern Border Fault, Connecticut [M.S.: University of Massachusetts, 109 p.
Saunders, A., Jones, S., Morgan, L., Pierce, K., Widdowson, M., and Xu, Y., 2007, Regional uplift associated with continental large igneous provinces: the roles of mantle plumes and the lithosphere: Chemical Geology, v. 241, no. 3, p. 282-318.
Sawyer, J., and Carroll, S. E., 1982, Fracture deformation of the Higganum dike, south-central Connecticut: Nuclear Regulatory Commission
Schlische, R. W., 1995, Geometry and origin of fault-related folds in extensional settings: AAPG bulletin, v. 79, no. 11, p. 1661-1678.
Schoene, B., Guex, J., Bartolini, A., Schaltegger, U., and Blackburn, T. J., 2010, Correlating the end-Triassic mass extinction and flood basalt volcanism at the 100 ka level: Geology, v. 38, no. 5, p. 387-390.
Silver, P. G., Behn, M. D., Kelley, K., Schmitz, M., and Savage, B., 2006, Understanding cratonic flood basalts: Earth and Planetary Science Letters, v. 245, no. 1, p. 190-201.
Sperner, B., and Zweigel, P., 2010, A plea for more caution in fault–slip analysis: Tectonophysics, v. 482, no. 1, p. 29-41.
Sue, C., Le Gall, B., and Daoud, A. M., 2014, Stress field during early magmatism in the Ali Sabieh Dome, Djibouti, SE Afar rift: Journal of African Earth Sciences, v. 97, p. 56-66.
Wallace, R. E., 1951, Geometry of shearing stress and relation to faulting: The Journal of Geology, p. 118-130.
Wise, D., and Robinson, P., Tectonics of the Mesozoic Connecticut Valley graben, *in* Proceedings Geol. Soc. Am. Abstr. Programs1982, Volume 14, p. 96.
Wise, D. U., 1981, Fault, fracture, and lineament date for western Massachusetts and western Connecticut, U.S. Nuclear Regulatory Commission, 253 p.:
Withjack, M. O., Baum, M. S., and Schlische, R. W., 2010, Influence of preexisting fault fabric on inversion-related deformation: A case study of the inverted Fundy rift basin, southeastern Canada: Tectonics, v. 29, no. 6.
Withjack, M. O., Olsen, P. E., and Schlische, R. W., 1995, Tectonic evolution of the Fundy rift basin, Canada: evidence of extension and shortening during passive margin development: Tectonics, v. 14, no. 2, p. 390-405.
Withjack, M. O., Schlische, R. W., and Olsen, P. E., 1998, Diachronous rifting, drifting, and inversion on the passive margin of central eastern North America: an analog for other passive margins: AAPG bulletin, v. 82, no. 5, p. 817-835.
-, 2012, Development of the passive margin of eastern North America: Mesozoic rifting, igneous activity, and breakup: Regional Geology and Tectonics: Phanerozoic Rift Systems and Sedimentary Basins: Phanerozoic Rift Systems and Sedimentary Basins, p. 301.
Woodward-Clyde, 1988, Moodus, Connecticut Borehole Research Project: the magnitude and orientation of tectonic stress in southern New England: Empire State Electric Energy Research Corporation, Northeast Utilities and Electric Power Institute.

Žalohar, J., and Vrabec, M., 2007, Paleostress analysis of heterogeneous fault-slip data: the Gauss method: Journal of structural Geology, v. 29, no. 11, p. 1798-1810.
Ziegler, P. A., and Cloetingh, S., 2004, Dynamic processes controlling evolution of rifted basins: Earth-Science Reviews, v. 64, no. 1, p. 1-50.
Zoback, M. L., 1992, Stress field constraints on intraplate seismicity in eastern North America: Journal of Geophysical Research: Solid Earth (1978–2012), v. 97, no. B8, p. 11761-11782.

APPENDIX A – Outcrop Locations

Outcrop	Location	State	Latitude(N)	Longitude(W)	Lithology1	Lithology2
HB1	Holyoke	MA	42.240564	72.623332	Portland	
HB2	Holyoke	MA	42.234185	72.628788	Holyoke	
HB3	Holyoke	MA	42.195339	72.6479	East Berlin	
HB4	Holyoke	MA	42.192766	72.648969	East Berlin	
HB5	Suffield	CT	42.004566	72.725498	Holyoke	
HB6	East Granby	CT	41.946678	72.739077	Holyoke	
HB7	Tariffville	CT	41.903213	72.761204	Holyoke	
HB8	Avon	CT	41.798299	72.802378	Talcott	
HB9	Avon	CT	41.796105	72.797467	Holyoke	
HB10	Avon	CT	41.793371	72.793407	Holyoke	
HB11	Farmington	CT	41.724238	72.807558	Holyoke	Talcott
HB12	Farmington	CT	41.716387	72.767554	East Berlin	
HB13	Farmington	CT	41.707719	72.815725	Holyoke	
HB14	Newington	CT	41.698337	72.710953	Holyoke	
HB15	Newington	CT	41.686959	72.706071	Holyoke	
HB16	Newington	CT	41.682697	72.706439	Holyoke	
HB17	Plainville	CT	41.67078	72.824218	Holyoke	
HB18	Plainville	CT	41.678648	72.821302	Holyoke	
HB19	Rocky Hill	CT	41.648963	72.664132	Hampden	
HB20	Rocky Hill	CT	41.648097	72.663082	Hampden	
HB21	Rocky Hill	CT	41.64678	72.669746	Hampden	

Outcrop	Location	State	Latitude(N)	Longitude(W)	Lithology1	Lithology2
HB22	Berlin	CT	41.623075	72.735026	Hampden	East Berlin
HB23	Berlin	CT	41.582313	72.762836	Talcott	
HB24	Cheshire	CT	41.515454	72.926041	West Rock	
HB25	Wallingford	CT	41.439882	72.848515	West Rock	
HB26	Hamden	CT	41.419721	72.904754	West Rock	
HB27	Hamden	CT	41.412134	72.90682	New Haven	
HB28	New Haven	CT	41.327665	72.864928	West Rock	
HB29	East Haven	CT	41.323147	72.856165	Buttress	

APPENDIX B – Fault Slip Data (This Study)

Fault	Outcrop	Strike	Dip	Rake	Sense	Lithology
1	HB1	018	47	106	N	Portland
2	HB1	025	74	122	N	Portland
3	HB1	008	54	115	N	Portland
4	HB1	016	70	116	N	Portland
5	HB2	224	83	27	S	Hampden
6	HB2	030	88	142	S	Hampden
7	HB2	204	70	91	N	Hampden
8	HB2	240	77	57	N	Hampden
9	HB3	019	80	101	N	East Berlin
10	HB3	038	64	99	N	East Berlin
11	HB4	032	62	88	N	East Berlin
12	HB5	178	84	40	S	Holyoke
13	HB5	141	77	26	S	Holyoke
14	HB5	151	89	172	S	Holyoke
15	HB5	160	62	163	D	Holyoke
16	HB5	142	66	167	S	Holyoke
17	HB5	175	64	100	N	Holyoke
18	HB5	166	71	174	D	Holyoke
19	HB5	181	72	100	N	Holyoke
20	HB5	181	78	171	D	Holyoke
21	HB6	136	77	103	N	Holyoke

Fault	Outcrop	Strike	Dip	Rake	Sense	Lithology
22	HB6	174	72	106	N	Holyoke
23	HB6	178	70	63	N	Holyoke
24	HB7	316	74	44	D	Holyoke
25	HB7	210	61	89	N	Holyoke
26	HB7	291	76	58	N	Holyoke
27	HB7	175	64	85	N	Holyoke
28	HB7	172	78	39	D	Holyoke
29	HB7	337	32	99	N	Holyoke
30	HB7	160	75	146	S	Holyoke
31	HB7	171	70	140	S	Holyoke
32	HB7	147	75	171	S	Holyoke
33	HB7	305	85	74	N	Holyoke
34	HB7	184	36	93	N	Holyoke
35	HB7	220	54	64	N	Holyoke
36	HB7	220	48	87	N	Holyoke
37	HB7	305	81	23	S	Holyoke
38	HB7	286	84	50	N	Holyoke
39	HB7	309	71	114	N	Holyoke
40	HB8	179	65	167	D	Talcott
41	HB8	165	59	11	D	Talcott
42	HB8	142	86	19	S	Talcott
43	HB8	155	70	12	S	Talcott

Fault	Outcrop	Strike	Dip	Rake	Sense	Lithology
44	HB8	152	76	16	D	Talcott
45	HB8	153	89	179	S	Talcott
46	HB8	179	82	23	D	Talcott
47	HB8	164	79	28	D	Talcott
48	HB9	148	86	174	D	Holyoke
49	HB9	318	89	8	S	Holyoke
50	HB9	325	86	176	D	Holyoke
51	HB9	170	82	84	N	Holyoke
52	HB9	185	66	91	N	Holyoke
53	HB9	181	89	85	N	Holyoke
54	HB9	144	84	173	S	Holyoke
55	HB9	330	89	6	D	Holyoke
56	HB9	154	74	177	D	Holyoke
57	HB10	040	82	8	S	Holyoke
58	HB10	034	85	177	S	Holyoke
59	HB10	031	59	10	D	Holyoke
60	HB10	208	80	2	S	Holyoke
61	HB10	214	87	170	S	Holyoke
62	HB10	005	85	7	S	Holyoke
63	HB10	205	85	178	S	Holyoke
64	HB10	026	80	10	S	Holyoke
65	HB10	194	89	177	S	Holyoke

Fault	Outcrop	Strike	Dip	Rake	Sense	Lithology
66	HB11	172	86	18	S	Holyoke
67	HB11	001	78	1	S	Holyoke
68	HB11	185	75	3	S	Holyoke
69	HB11	167	84	16	S	Holyoke
70	HB11	184	84	3	D	Holyoke
71	HB11	188	77	161	D	Holyoke
72	HB11	170	80	24	S	Holyoke
73	HB11	162	84	39	D	Holyoke
74	HB11	174	78	65	I	Holyoke
75	HB11	147	89	16	S	Holyoke
76	HB11	194	52	120	N	Holyoke
77	HB11	172	83	173	D	Holyoke
78	HB11	175	70	27	D	Holyoke
79	HB11	181	86	11	S	Holyoke
80	HB11	193	62	29	S	Holyoke
81	HB11	223	83	179	D	Holyoke
82	HB11	169	82	19	D	Holyoke
83	HB11	157	84	15	S	Holyoke
84	HB11	154	86	170	D	Holyoke
85	HB11	188	76	55	I	Holyoke
86	HB11	196	80	22	D	Holyoke
87	HB11	215	74	178	D	Holyoke

Fault	Outcrop	Strike	Dip	Rake	Sense	Lithology
88	HB11	163	88	14	S	Holyoke
89	HB11	165	89	169	S	Holyoke
90	HB11	203	78	150	S	Holyoke
91	HB11	214	57	115	I	Holyoke
92	HB11	209	60	142	S	Holyoke
93	HB11	212	59	132	I	Holyoke
94	HB11	340	79	179	S	Holyoke
95	HB11	211	64	46	N	Holyoke
96	HB11	192	82	10	D	Holyoke
97	HB11	225	78	152	D	Holyoke
98	HB11	220	68	161	D	Holyoke
99	HB11	053	86	25	D	Holyoke
100	HB11	191	77	11	D	Holyoke
101	HB11	219	85	175	D	Holyoke
102	HB11	291	33	114	N	Holyoke
103	HB11	002	88	179	S	Holyoke
104	HB11	179	86	5	S	Talcott
105	HB11	167	89	170	S	Talcott
106	HB11	155	79	4	S	Talcott
107	HB11	216	81	8	S	Talcott
108	HB11	205	84	17	S	Talcott
109	HB11	230	41	120	N	Talcott

Fault	Outcrop	Strike	Dip	Rake	Sense	Lithology
110	HB11	005	88	1	D	Talcott
111	HB11	357	87	47	N	Talcott
112	HB11	193	70	172	D	Talcott
113	HB11	200	83	30	D	Talcott
114	HB11	216	86	3	S	Talcott
115	HB11	207	67	117	N	Talcott
116	HB11	210	89	31	D	Talcott
117	HB11	217	83	22	D	Talcott
118	HB11	210	81	10	S	Talcott
119	HB11	214	81	12	D	Talcott
120	HB11	216	87	48	I	Talcott
121	HB11	216	87	20	S	Talcott
122	HB11	214	77	11	D	Talcott
123	HB11	215	89	88	N	Talcott
124	HB11	166	89	162	D	Talcott
125	HB11	220	78	12	D	Holyoke
126	HB11	188	84	179	D	Holyoke
127	HB11	357	86	1	D	Holyoke
128	HB11	261	85	165	D	Holyoke
129	HB11	230	79	169	S	Holyoke
130	HB11	234	82	172	S	Holyoke
131	HB11	001	78	172	D	Holyoke

Fault	Outcrop	Strike	Dip	Rake	Sense	Lithology
132	HB11	241	80	170	D	Holyoke
133	HB11	251	72	171	D	Holyoke
134	HB11	232	82	175	D	Holyoke
135	HB11	252	79	178	D	Holyoke
136	HB11	255	82	177	D	Holyoke
137	HB11	216	81	20	D	Holyoke
138	HB11	248	74	156	D	Holyoke
139	HB12	215	86	89	N	East Berlin
140	HB12	210	81	80	N	East Berlin
141	HB12	020	83	114	N	East Berlin
142	HB12	207	86	9	D	East Berlin
143	HB12	019	71	96	N	East Berlin
144	HB12	022	67	97	N	East Berlin
145	HB12	197	86	172	D	East Berlin
146	HB12	199	86	16	S	East Berlin
147	HB12	211	83	94	N	East Berlin
148	HB12	210	73	64	N	East Berlin
149	HB12	049	53	79	N	East Berlin
150	HB12	192	89	13	S	East Berlin
151	HB12	196	41	116	N	East Berlin
152	HB12	015	72	99	N	East Berlin
153	HB12	206	61	95	N	East Berlin

Fault	Outcrop	Strike	Dip	Rake	Sense	Lithology
154	HB12	020	69	87	N	East Berlin
155	HB12	015	65	94	N	East Berlin
156	HB12	031	69	80	N	East Berlin
157	HB12	195	72	129	N	East Berlin
158	HB12	206	55	101	N	East Berlin
159	HB12	197	56	102	N	East Berlin
160	HB12	189	52	100	N	East Berlin
161	HB12	011	68	95	N	East Berlin
162	HB12	202	59	92	N	East Berlin
163	HB12	187	60	96	N	East Berlin
164	HB12	014	65	111	N	East Berlin
165	HB12	012	51	100	N	East Berlin
166	HB12	202	44	91	N	East Berlin
167	HB12	036	75	79	N	East Berlin
168	HB12	204	56	79	N	East Berlin
169	HB12	026	76	81	N	East Berlin
170	HB12	012	66	99	N	East Berlin
171	HB12	018	65	99	N	East Berlin
172	HB12	012	76	95	N	East Berlin
173	HB13	044	89	156	D	Holyoke
174	HB13	059	85	167	D	Holyoke
175	HB13	011	75	21	S	Holyoke

Fault	Outcrop	Strike	Dip	Rake	Sense	Lithology
176	HB13	046	79	6	D	Holyoke
177	HB13	056	89	158	D	Holyoke
178	HB13	359	80	9	S	Holyoke
179	HB13	048	82	160	D	Holyoke
180	HB13	261	88	2	S	Holyoke
181	HB13	043	79	156	D	Holyoke
182	HB13	237	87	16	S	Holyoke
183	HB13	254	84	14	S	Holyoke
184	HB13	204	83	155	D	Holyoke
185	HB13	182	88	3	S	Holyoke
186	HB13	196	64	161	D	Holyoke
187	HB13	236	77	14	S	Holyoke
188	HB14	338	88	164	S	Holyoke
189	HB14	217	75	80	N	Holyoke
190	HB14	129	71	7	S	Holyoke
191	HB14	148	82	10	D	Holyoke
192	HB14	134	89	3	S	Holyoke
193	HB14	140	77	121	N	Holyoke
194	HB14	198	71	77	N	Holyoke
195	HB14	073	56	76	N	Holyoke
196	HB14	351	78	149	S	Holyoke
197	HB14	154	64	25	S	Holyoke

Fault	Outcrop	Strike	Dip	Rake	Sense	Lithology
198	HB14	163	84	27	S	Holyoke
199	HB14	127	89	33	D	Holyoke
200	HB14	144	84	15	D	Holyoke
201	HB14	149	78	1	S	Holyoke
202	HB14	147	57	81	N	Holyoke
203	HB14	282	81	26	S	Holyoke
204	HB14	308	83	150	D	Holyoke
205	HB14	120	81	175	D	Holyoke
206	HB14	275	78	146	D	Holyoke
207	HB14	096	88	17	D	Holyoke
208	HB14	095	89	18	D	Holyoke
209	HB14	273	84	172	D	Holyoke
210	HB15	147	87	17	S	Holyoke
211	HB15	156	88	10	D	Holyoke
212	HB15	311	82	175	S	Holyoke
213	HB15	183	68	20	S	Holyoke
214	HB15	339	83	174	D	Holyoke
215	HB15	174	81	168	D	Holyoke
216	HB15	333	77	154	S	Holyoke
217	HB15	335	77	168	D	Holyoke
218	HB15	002	89	115	N	Holyoke
219	HB15	323	85	160	D	Holyoke

Fault	Outcrop	Strike	Dip	Rake	Sense	Lithology
220	HB15	332	89	168	D	Holyoke
221	HB15	355	81	142	D	Holyoke
222	HB15	332	68	164	D	Holyoke
223	HB15	345	89	162	D	Holyoke
224	HB15	324	86	172	D	Holyoke
225	HB15	304	83	179	S	Holyoke
226	HB15	316	89	173	D	Holyoke
227	HB15	316	78	175	S	Holyoke
228	HB15	340	87	163	D	Holyoke
229	HB15	312	82	4	S	Holyoke
230	HB15	301	88	164	S	Holyoke
231	HB15	324	50	177	D	Holyoke
232	HB15	347	80	49	N	Holyoke
233	HB15	015	82	171	S	Holyoke
234	HB15	322	78	172	D	Holyoke
235	HB15	029	89	162	S	Holyoke
236	HB15	304	76	175	D	Holyoke
237	HB15	331	72	168	S	Holyoke
238	HB15	174	71	13	S	Holyoke
239	HB15	009	85	166	S	Holyoke
240	HB15	036	75	153	D	Holyoke
241	HB15	200	84	14	S	Holyoke

Fault	Outcrop	Strike	Dip	Rake	Sense	Lithology
242	HB15	184	88	53	N	Holyoke
243	HB15	182	88	55	N	Holyoke
244	HB15	179	84	160	D	Holyoke
245	HB15	181	81	26	S	Holyoke
246	HB15	186	78	20	S	Holyoke
247	HB15	211	80	21	S	Holyoke
248	HB15	143	83	2	D	Holyoke
249	HB15	199	87	172	S	Holyoke
250	HB15	165	89	12	D	Holyoke
251	HB15	187	87	19	S	Holyoke
252	HB15	348	76	41	D	Holyoke
253	HB15	192	85	19	S	Holyoke
254	HB15	218	87	169	D	Holyoke
255	HB15	179	84	10	S	Holyoke
256	HB15	200	85	7	D	Holyoke
257	HB15	181	79	30	S	Holyoke
258	HB15	193	76	4	D	Holyoke
259	HB15	187	83	37	S	Holyoke
260	HB15	022	84	157	S	Holyoke
261	HB15	025	87	174	S	Holyoke
262	HB15	178	89	26	D	Holyoke
263	HB15	134	84	20	S	Holyoke

Fault	Outcrop	Strike	Dip	Rake	Sense	Lithology
264	HB15	147	88	14	D	Holyoke
265	HB15	204	82	176	S	Holyoke
266	HB15	332	52	141	D	Holyoke
267	HB15	149	89	14	D	Holyoke
268	HB15	312	80	158	D	Holyoke
269	HB15	320	88	147	D	Holyoke
270	HB15	350	86	172	D	Holyoke
271	HB15	164	84	7	D	Holyoke
272	HB15	191	80	25	S	Holyoke
273	HB15	148	84	19	D	Holyoke
274	HB15	201	69	44	S	Holyoke
275	HB15	183	84	81	N	Holyoke
276	HB15	176	74	61	N	Holyoke
277	HB15	178	66	71	N	Holyoke
278	HB15	206	81	11	S	Holyoke
279	HB15	211	68	21	D	Holyoke
280	HB15	216	79	32	D	Holyoke
281	HB15	172	69	41	S	Holyoke
282	HB15	184	76	50	N	Holyoke
283	HB15	201	71	49	N	Holyoke
284	HB15	186	64	57	N	Holyoke
285	HB15	351	86	167	S	Holyoke

Fault	Outcrop	Strike	Dip	Rake	Sense	Lithology
286	HB15	181	83	13	S	Holyoke
287	HB15	179	85	12	S	Holyoke
288	HB15	020	79	9	S	Holyoke
289	HB15	179	74	35	S	Holyoke
290	HB15	181	89	34	S	Holyoke
291	HB15	157	89	155	D	Holyoke
292	HB15	198	76	29	S	Holyoke
293	HB15	216	82	16	S	Holyoke
294	HB15	210	86	11	S	Holyoke
295	HB15	027	85	13	S	Holyoke
296	HB15	188	80	4	S	Holyoke
297	HB15	194	79	38	S	Holyoke
298	HB15	226	69	15	S	Holyoke
299	HB15	203	79	31	D	Holyoke
300	HB15	192	80	31	S	Holyoke
301	HB15	023	85	171	S	Holyoke
302	HB15	147	86	178	D	Holyoke
303	HB15	205	76	16	S	Holyoke
304	HB15	215	78	12	D	Holyoke
305	HB15	211	89	19	S	Holyoke
306	HB15	227	86	179	D	Holyoke
307	HB15	209	76	14	S	Holyoke

Fault	Outcrop	Strike	Dip	Rake	Sense	Lithology
308	HB15	191	83	25	S	Holyoke
309	HB15	206	86	7	D	Holyoke
310	HB15	184	89	26	S	Holyoke
311	HB15	192	84	14	S	Holyoke
312	HB15	311	79	2	S	Holyoke
313	HB15	191	76	23	S	Holyoke
314	HB15	197	88	12	S	Holyoke
315	HB15	181	74	17	S	Holyoke
316	HB15	324	81	165	D	Holyoke
317	HB15	134	74	178	D	Holyoke
318	HB15	201	89	9	S	Holyoke
319	HB15	319	86	170	S	Holyoke
320	HB15	204	75	175	S	Holyoke
321	HB15	181	74	150	D	Holyoke
322	HB15	170	83	166	D	Holyoke
323	HB15	173	86	154	D	Holyoke
324	HB15	173	74	54	N	Holyoke
325	HB15	182	89	36	S	Holyoke
326	HB15	174	86	55	N	Holyoke
327	HB15	181	81	40	S	Holyoke
328	HB15	175	80	71	N	Holyoke
329	HB15	154	84	11	D	Holyoke

Fault	Outcrop	Strike	Dip	Rake	Sense	Lithology
330	HB15	203	76	4	S	Holyoke
331	HB15	202	71	30	S	Holyoke
332	HB15	316	76	1	D	Holyoke
333	HB15	266	68	88	N	Holyoke
334	HB15	146	89	19	D	Holyoke
335	HB15	292	84	163	D	Holyoke
336	HB15	295	83	40	D	Holyoke
337	HB15	204	73	21	S	Holyoke
338	HB16	217	89	6	D	Holyoke
339	HB16	213	76	94	N	Holyoke
340	HB16	192	76	91	N	Holyoke
341	HB16	172	55	104	N	Holyoke
342	HB16	195	74	81	N	Holyoke
343	HB16	051	84	91	N	Holyoke
344	HB16	349	75	76	N	Holyoke
345	HB16	009	89	125	N	Holyoke
346	HB16	034	59	76	N	Holyoke
347	HB16	203	83	96	N	Holyoke
348	HB16	209	85	75	N	Holyoke
349	HB16	215	88	31	D	Holyoke
350	HB16	334	89	9	S	Holyoke
351	HB16	333	89	10	D	Holyoke

Fault	Outcrop	Strike	Dip	Rake	Sense	Lithology
352	HB16	349	81	11	S	Holyoke
353	HB16	346	65	42	D	Holyoke
354	HB16	147	78	129	D	Holyoke
355	HB16	346	68	98	N	Holyoke
356	HB16	215	87	142	D	Holyoke
357	HB16	181	86	147	D	Holyoke
358	HB16	216	89	165	S	Holyoke
359	HB16	271	44	117	N	Holyoke
360	HB16	262	44	103	N	Holyoke
361	HB16	228	36	166	D	Holyoke
362	HB16	191	81	84	N	Holyoke
363	HB16	223	61	71	N	Holyoke
364	HB16	216	61	66	N	Holyoke
365	HB16	215	57	73	N	Holyoke
366	HB16	199	84	179	D	Holyoke
367	HB16	211	53	94	N	Holyoke
368	HB16	197	54	126	N	Holyoke
369	HB16	334	84	165	D	Holyoke
370	HB16	334	87	177	S	Holyoke
371	HB16	218	61	84	N	Holyoke
372	HB16	202	62	175	D	Holyoke
373	HB16	241	61	66	N	Holyoke

Fault	Outcrop	Strike	Dip	Rake	Sense	Lithology
374	HB16	246	65	72	N	Holyoke
375	HB16	181	58	110	N	Holyoke
376	HB16	179	88	179	D	Holyoke
377	HB17	060	79	154	D	Holyoke
378	HB17	223	84	153	D	Holyoke
379	HB17	347	14	51	N	Holyoke
380	HB17	210	89	172	D	Holyoke
381	HB17	220	81	161	D	Holyoke
382	HB17	192	84	168	S	Holyoke
383	HB17	188	89	156	S	Holyoke
384	HB17	192	83	163	S	Holyoke
385	HB18	078	81	18	D	Holyoke
386	HB18	084	64	8	D	Holyoke
387	HB18	099	89	12	D	Holyoke
388	HB18	040	80	6	S	Holyoke
389	HB18	265	88	37	D	Holyoke
390	HB18	048	89	10	S	Holyoke
391	HB18	089	70	152	D	Holyoke
392	HB18	081	79	145	D	Holyoke
393	HB18	032	84	13	S	Holyoke
394	HB18	029	54	21	S	Holyoke
395	HB18	357	61	40	S	Holyoke

Fault	Outcrop	Strike	Dip	Rake	Sense	Lithology
396	HB18	175	89	145	S	Holyoke
397	HB18	048	46	179	D	Holyoke
398	HB18	052	60	158	D	Holyoke
399	HB18	041	45	165	D	Holyoke
400	HB18	050	80	147	D	Holyoke
401	HB18	035	80	156	S	Holyoke
402	HB18	262	48	145	D	Holyoke
403	HB18	340	74	27	S	Holyoke
404	HB18	043	70	5	S	Holyoke
405	HB18	070	70	155	D	Holyoke
406	HB18	024	70	24	S	Holyoke
407	HB18	021	75	19	S	Holyoke
408	HB18	019	78	20	S	Holyoke
409	HB18	035	71	9	S	Holyoke
410	HB18	059	89	27	D	Holyoke
411	HB18	057	76	155	D	Holyoke
412	HB18	280	86	165	D	Holyoke
413	HB18	230	80	175	D	Holyoke
414	HB18	039	80	177	S	Holyoke
415	HB18	020	88	7	S	Holyoke
416	HB18	051	69	165	S	Holyoke
417	HB18	026	83	163	S	Holyoke

Fault	Outcrop	Strike	Dip	Rake	Sense	Lithology
418	HB18	179	85	1	S	Holyoke
419	HB18	036	75	31	S	Holyoke
420	HB18	031	72	29	D	Holyoke
421	HB18	211	89	169	D	Holyoke
422	HB18	031	83	7	D	Holyoke
423	HB18	212	85	170	D	Holyoke
424	HB18	212	87	3	D	Holyoke
425	HB18	209	89	6	D	Holyoke
426	HB18	030	79	179	D	Holyoke
427	HB18	028	83	175	D	Holyoke
428	HB18	211	85	9	D	Holyoke
429	HB18	030	82	5	D	Holyoke
430	HB18	031	89	176	D	Holyoke
431	HB18	030	89	2	D	Holyoke
432	HB18	029	88	179	D	Holyoke
433	HB18	206	84	179	S	Holyoke
434	HB19	219	78	7	D	Hampden
435	HB19	281	88	171	D	Hampden
436	HB19	021	82	2	S	Hampden
437	HB19	219	82	168	S	Hampden
438	HB19	209	80	1	S	Hampden
439	HB19	044	79	2	D	Hampden

Fault	Outcrop	Strike	Dip	Rake	Sense	Lithology
440	HB19	227	79	165	D	Hampden
441	HB20	268	70	3	D	Hampden
442	HB21	021	88	2	D	Hampden
443	HB21	197	89	164	D	Hampden
444	HB21	189	86	6	S	Hampden
445	HB21	247	82	3	S	Hampden
446	HB21	046	84	2	S	Hampden
447	HB22	114	42	105	N	Hampden
448	HB22	251	86	170	D	Hampden
449	HB23	176	63	136	N	Talcott
450	HB23	247	73	142	S	Talcott
451	HB23	249	86	155	D	Talcott
452	HB23	240	74	161	S	Talcott
453	HB23	265	80	145	S	Talcott
454	HB23	065	89	18	S	Talcott
455	HB23	231	83	167	S	Talcott
456	HB23	244	71	167	S	Talcott
457	HB23	246	61	172	S	Talcott
458	HB23	246	75	8	S	Talcott
459	HB23	244	74	173	S	Talcott
460	HB23	252	81	178	S	Talcott
461	HB23	256	78	22	S	Talcott

Fault	Outcrop	Strike	Dip	Rake	Sense	Lithology
462	HB23	249	66	174	S	Talcott
463	HB24	320	81	138	S	West Rock
464	HB24	202	60	68	N	West Rock
465	HB24	306	81	149	S	West Rock
466	HB24	311	79	155	S	West Rock
467	HB24	050	81	152	D	West Rock
468	HB24	311	82	138	S	West Rock
469	HB24	029	47	145	S	West Rock
470	HB24	055	71	165	D	West Rock
471	HB24	034	61	151	D	West Rock
472	HB24	110	68	105	N	West Rock
473	HB24	268	69	24	D	West Rock
474	HB24	111	85	76	N	West Rock
475	HB24	334	84	161	S	West Rock
476	HB24	334	81	25	S	West Rock
477	HB24	117	89	72	N	West Rock
478	HB24	335	85	108	N	West Rock
479	HB24	127	89	34	S	West Rock
480	HB24	272	77	41	D	West Rock
481	HB24	321	86	106	N	West Rock
482	HB24	182	59	31	S	West Rock
483	HB24	316	84	36	D	West Rock

Fault	Outcrop	Strike	Dip	Rake	Sense	Lithology
484	HB24	314	76	47	N	West Rock
485	HB24	156	66	168	S	West Rock
486	HB24	137	86	21	S	West Rock
487	HB24	277	73	42	D	West Rock
488	HB24	152	78	20	S	West Rock
489	HB24	146	82	38	S	West Rock
490	HB24	130	89	31	S	West Rock
491	HB24	251	78	71	N	West Rock
492	HB24	236	58	167	D	West Rock
493	HB24	134	81	34	S	West Rock
494	HB24	124	87	44	S	West Rock
495	HB25	010	88	15	S	West Rock
496	HB25	199	81	164	S	West Rock
497	HB25	170	81	161	S	West Rock
498	HB25	126	75	159	D	West Rock
499	HB25	111	86	21	D	West Rock
500	HB25	331	79	14	S	West Rock
501	HB25	114	88	20	D	West Rock
502	HB25	125	86	141	D	West Rock
503	HB25	016	88	34	S	West Rock
504	HB25	114	76	164	D	West Rock
505	HB25	104	78	159	D	West Rock

Fault	Outcrop	Strike	Dip	Rake	Sense	Lithology
506	HB25	136	87	169	D	West Rock
507	HB25	096	81	153	D	West Rock
508	HB25	122	82	169	D	West Rock
509	HB25	104	82	179	D	West Rock
510	HB25	279	82	1	D	West Rock
511	HB25	105	78	176	D	West Rock
512	HB25	127	87	149	D	West Rock
513	HB25	278	88	150	D	West Rock
514	HB25	283	89	1	D	West Rock
515	HB25	115	78	44	D	West Rock
516	HB25	230	61	83	N	West Rock
517	HB25	114	81	166	D	West Rock
518	HB26	181	89	155	S	West Rock
519	HB26	021	88	68	N	West Rock
520	HB26	021	87	98	N	West Rock
521	HB26	019	75	99	N	West Rock
522	HB26	198	81	110	N	West Rock
523	HB26	030	86	66	N	West Rock
524	HB27	210	81	83	N	New Haven
525	HB27	035	75	79	N	New Haven
526	HB27	034	66	80	N	New Haven
527	HB27	208	83	89	N	New Haven

Fault	Outcrop	Strike	Dip	Rake	Sense	Lithology
528	HB28	214	53	96	N	West Rock
529	HB28	229	82	56	N	West Rock
530	HB28	178	74	59	N	West Rock
531	HB28	241	89	72	N	West Rock
532	HB28	166	43	57	N	West Rock
533	HB28	183	61	39	S	West Rock
534	HB28	016	74	104	N	West Rock
535	HB28	059	82	101	N	West Rock
536	HB28	049	80	130	N	West Rock
537	HB28	040	87	88	N	West Rock
538	HB29	253	82	108	N	Buttress

APPENDIX C – Fault Slip Data (Clifton, 1987 – original key)

Fault	Outcrop	Strike	Dip	Rake	Sense	Lithology
NE78	5f	027	70	80	N	Bord
NE79	5f	038	64	130	D	Bord
NE80	5f	046	83	85	N	Bord
NE83	5f	034	62	90	N	Bord
NE89	5f	038	58	90	N	Bord
NE90	5f	027	67	90	N	Bord
NE91	5f	041	71	90	N	Bord
NE92	5f	020	71	90	N	Bord
NE94	5f	066	48	80	N	Bord
NS62	5f	012	61	100	N	Bord
NS63	5f	002	76	90	N	Bord
NS64	5f	016	75	90	N	Bord
NS65	5f	005	72	90	N	Bord
NS66	5f	010	70	90	N	Bord
NS70	5f	019	67	122	D	Bord
NS71	5f	192	55	95	N	Bord
NS72	5f	015	83	115	N	Bord
NS73	5f	170	90	102	N	Bord
NS74	5f	004	75	90	N	Bord
NS76	5f	009	73	123	D	Bord
NS77	5f	017	80	135	D	Bord

Fault	Outcrop	Strike	Dip	Rake	Sense	Lithology
NS78	5f	184	86	85	N	Bord
NS79	5f	194	64	100	N	Bord
NS80	5f	016	76	110	N	Bord
EW53	5f	072	65	90	N	Bord
EW54	5f	078	70	90	N	Bord
EW55	5f	095	66	90	N	Bord
EW56	5f	073	52	90	N	Bord
EW57	5f	089	52	90	N	Bord
NW52	5f	112	56	90	N	Bord
NW53	5f	322	80	95	N	Bord
NW54	5f	324	82	85	N	Bord
NW55	5f	301	72	115	N	Bord
NW49	5e	150	88	58	S	Ark
NW50	5e	334	76	165	S	Ark
NE86	5c	037	25	55	S	Ark
NE87	5c	223	47	96	N	Ark
NE88	5c	206	49	105	N	Ark
NS57	5c	015	32	40	S	Ark
NS58	5c	005	49	70	N	Ark
NW51	5c	110	54	68	N	Ark
NE84	5b	060	81	90	N	Ark
NE85	5b	220	65	90	N	Ark

Fault	Outcrop	Strike	Dip	Rake	Sense	Lithology
NE93	5b	213	30	67	N	Ark
NS56	5b	175	54	100	N	Ark
NS81	5b	180	65	172	D	Ark
EW48	5b	089	50	90	N	Ark
EW49	5b	102	68	90	N	Ark
EW58	5b	094	60	90	N	Ark
NE41	4j	052	55	52	S	Ark
NE42	4j	026	75	95	N	Ark
NE43	4j	026	75	45	S	Ark
NE44	4j	066	55	87	N	Ark
NE45	4j	066	55	119	N	Ark
NE57	4j	210	62	45	S	Ark
NE58	4j	067	41	113	N	Ark
NE59	4j	070	57	84	N	Ark
NE60	4j	065	56	114	N	Ark
NE72	4j	210	54	45	S	Ark
NE73	4j	209	61	35	I	Ark
NE74	4j	215	62	42	D	Ark
NE75	4j	216	87	10	D	Ark
NE76	4j	030	30	90	N	Ark
NS35	4j	017	80	15	D	Ark
NS42	4j	011	83	88	N	Ark

Fault	Outcrop	Strike	Dip	Rake	Sense	Lithology
NS43	4j	186	73	165	D	Ark
NS44	4j	018	76	20	D	Ark
NS45	4j	193	82	170	D	Ark
NS46	4j	010	43	77	N	Ark
NS49	4j	005	90	47	S	Ark
NS50	4j	015	65	90	N	Ark
NS51	4j	000	80	111	N	Ark
NS52	4j	200	55	60	N	Ark
NS53	4j	010	80	88	N	Ark
NS54	4j	010	75	108	N	Ark
NS55	4j	198	55	60	N	Ark
EW33	4j	285	46	75	N	Ark
EW34	4j	285	40	97	N	Ark
EW42	4j	272	54	114	N	Ark
EW43	4j	290	44	70	N	Ark
EW44	4j	081	49	90	N	Ark
EW45	4j	283	46	78	N	Ark
NW47	4j	297	53	71	N	Ark
NS36	4h	358	87	73	N	Ark
NS41	4h	020	75	80	N	Ark
NE61	4g	220	32	40	S	Diab
NS37	4g	196	60	60	N	Diab

Fault	Outcrop	Strike	Dip	Rake	Sense	Lithology
NS48	4g	172	53	80	N	Diab
EW35	4g	080	87	105	N	Diab
EW36	4g	087	82	134	S	Diab
EW37	4g	082	86	133	D	Diab
EW38	4g	087	84	129	D	Diab
NE50	4d	236	88	0	S	Diab
NE55	4d	220	75	115	N	Diab
NS38	4d	168	62	145	D	Diab
NS39	4d	175	76	132	D	Diab
NE30	4c	238	79	125	D	Diab
NE31	4c	062	84	30	S	Diab
NE32	4c	237	83	25	S	Diab
NE34	4c	250	83	132	D	Diab
NE35	4c	236	70	150	D	Diab
NE37	4c	224	75	133	D	Diab
NE46	4c	062	82	90	N	Diab
NE47	4c	062	82	40	S	Diab
NE48	4c	020	76	50	S	Diab
NE49	4c	244	79	150	D	Diab
NS32	4c	178	65	140	D	Diab
NS33	4c	197	74	170	S	Diab
NS34	4c	165	78	142	D	Diab

Fault	Outcrop	Strike	Dip	Rake	Sense	Lithology
EW31	4c	108	87	60	N	Diab
EW32	4c	269	83	129	D	Diab
NW39	4c	157	70	9	S	Diab
NW42	4c	150	54	62	N	Diab
NW43	4c	149	81	162	S	Diab
NW44	4c	142	86	160	D	Diab
NW45	4c	154	50	67	N	Diab
NW46	4c	150	62	68	N	Diab
NE36	4b	247	82	129	D	Diab
NE51	4b	201	71	0	D	Diab
NE52	4b	201	71	0	S	Diab
NE53	4b	220	84	0	D	Diab
NE54	4b	220	84	0	S	Diab
EW39	4b	075	84	0	S	Diab
EW40	4b	072	82	0	S	Diab
NW37	4b	149	64	67	N	Diab
NW40	4b	142	62	30	S	Diab
NW41	4b	142	62	70	N	Diab
NS12	3d	005	56	130	D	Ark
NS28	3d	350	64	137	D	Ark
NE1	3c	035	72	110	N	Ark
NE2	3c	033	83	73	N	Ark

Fault	Outcrop	Strike	Dip	Rake	Sense	Lithology
NE3	3c	033	83	120	N	Ark
NE8	3c	027	74	158	D	Ark
NE9	3c	041	62	90	N	Ark
NE10	3c	028	63	90	N	Ark
NE11	3c	074	64	90	N	Ark
NE12	3c	208	79	14	D	Ark
NE13	3c	208	79	110	N	Ark
NS13	3c	359	79	170	D	Ark
NS14	3c	356	76	175	D	Ark
NS15	3c	170	74	120	N	Ark
NS20	3c	005	89	138	D	Ark
NS21	3c	016	86	115	N	Ark
NS23	3c	019	79	90	N	Ark
NS24	3c	006	81	90	N	Ark
NS25	3c	345	30	146	D	Ark
NS29	3c	018	82	108	N	Ark
NE4	3b	030	82	120	N	Ark
NE20	3b	226	76	115	N	Ark
NE24	3b	030	82	120	N	Ark
NS17	3b	010	51	100	N	Ark
NS26	3b	015	63	98	N	Ark
NS31	3b	015	63	98	N	Ark

Fault	Outcrop	Strike	Dip	Rake	Sense	Lithology
NE5	3a	222	80	138	D	Ark
NE6	3a	222	80	23	S	Ark
NE104	1e	040	90	65	D	Bas
NE105	1e	030	44	122	D	Ark
NE106	1e	042	72	105	N	Ark
NE107	1e	037	39	122	D	Ark
NE108	1e	247	61	43	S	Ark
NE109	1e	047	47	124	D	Ark
NE110	1e	220	67	73	N	Ark
NS1	1e	196	52	88	N	Ark
NS5	1e	160	50	118	N	Ark
NS6	1e	349	82	50	S	Diab
NS7	1e	170	31	90	N	Ark
NS8	1e	199	25	90	N	Ark
NS9	1e	183	40	90	N	Ark
NS10	1e	341	80	5	S	Ark
NS11	1e	358	70	129	D	Ark
EW7	1e	252	62	50	I	Ark
EW8	1e	285	72	85	N	Ark
EW9	1e	250	84	88	N	Ark
EW10	1e	085	84	90	N	Ark
EW11	1e	250	83	134	D	Ark

Fault	Outcrop	Strike	Dip	Rake	Sense	Lithology
EW12	1e	086	67	93	N	Ark
EW13	1e	074	85	93	N	Ark
EW14	1e	092	88	93	N	Ark
EW15	1e	267	88	90	N	Ark
EW16	1e	285	74	90	N	Ark
EW17	1e	272	74	87	N	Ark
NW3	1e	146	45	68	N	Ark
NW4	1e	146	45	135	D	Ark
NW5	1e	155	50	123	D	Ark
NW6	1e	156	67	95	N	Ark
NW7	1e	143	42	130	D	Ark
NW8	1e	310	84	90	N	Ark
NW9	1e	315	90	90	N	Diab
NW10	1e	140	38	133	D	Ark
NW11	1e	110	85	130	D	Ark
NW12	1e	145	39	48	S	Ark
NW13	1e	145	39	123	D	Ark
NW14	1e	138	42	12	D	Ark
NW15	1e	140	39	50	S	Ark
NW16	1e	140	39	140	D	Ark
NW17	1e	145	42	10	D	Ark
NW18	1e	156	57	120	N	Ark

Fault	Outcrop	Strike	Dip	Rake	Sense	Lithology
NW19	1e	153	40	142	D	Ark
NW20	1e	125	38	157	D	Ark
NW21	1e	128	48	144	D	Ark
NW22	1e	143	38	70	N	Ark
NW23	1e	143	38	130	D	Ark
NW24	1e	145	40	130	D	Ark
NW25	1e	145	40	155	D	Ark
NW26	1e	142	42	64	N	Ark
NW27	1e	142	42	143	D	Ark
NW28	1e	127	44	82	N	Ark
NW29	1e	127	44	163	D	Ark
NW30	1e	135	30	72	N	Ark
NW31	1e	135	30	165	D	Ark
NW32	1e	147	45	62	N	Ark
NE95	1d	237	34	120	N	Ark
NE96	1d	235	90	150	D	Ark
NE97	1d	232	75	88	N	Ark
NE98	1d	042	62	92	N	Ark
NS82	1d	340	40	110	N	Ark
NS83	1d	195	54	77	N	Ark
NS84	1d	358	79	90	N	Ark
NS85	1d	016	47	97	N	Ark

Fault	Outcrop	Strike	Dip	Rake	Sense	Lithology
NS86	1d	003	76	80	N	Ark
NS87	1d	184	60	72	N	Ark
NE112	1c	040	87	90	N	Ark
NE113	1c	062	59	40	S	Ark
EW4	1c	075	65	40	S	Ark

APPENDIX D – Software Parameters for T-Tecto Analysis

Guided Inversion - All values at default unless listed

Phase	S1	S3	q1	q2	Stress parameter	Dispersions
Phase 1	90	122	60	35	250	Large
Phase 2a	33	NA	60	35	250	Large
Phase 2b	0	NA	60	35	250	Large
Phase 3	NA	NA	60	35	250	Large
Phase 4	73	NA	60	35	250	Large

Blind Inversion – All values at default unless listed

Phase	S1	S3	q1	q2	Stress parameter	Dispersions
Phase 1	NA	NA	60	35	250	Large
Phase 2a	NA	NA	60	35	250	Large
Phase 2b	NA	NA	60	35	250	Large
Phase 3	NA	NA	60	35	250	Large
Phase 4	NA	NA	60	35	250	Large